NASA TECHNICAL MEMORANDUM

NASA TM X-73980

NASA TM X-73980

CONSIDERATIONS FOR THE APPLICATION OF FINITE-ELEMENT BEAM MODELING TO VIBRATION ANALYSIS OF FLIGHT VEHICLE STRUCTURES

Raymond G. Kvaternik
NASA-Langley Research Center
Hampton, Virginia 23665

November 1976

National Aeronautics and Space Administration

Langley Research Center
Hampton, Virginia 23665

1. Report No.	2. Government Accession No.	3. Recipient's Catalog No.
NASA TM X- 73980		

4. Title and Subtitle	5. Report Date
CONSIDERATIONS FOR THE APPLICATION OF FINITE-ELEMENT BEAM MODELING TO VIBRATION ANALYSIS OF FLIGHT VEHICLE STRUCTURES	November 1976
	6. Performing Organization Code

7. Author(s)	8. Performing Organization Report No.
Raymond G. Kvaternik	
	10. Work Unit No.
	505-10-26-01

9. Performing Organization Name and Address	11. Contract or Grant No.
NASA Langley Research Center Hampton, Va. 23665	
	13. Type of Report and Period Covered
	Technical Memorandum

12. Sponsoring Agency Name and Address	14. Sponsoring Agency Code
National Aeronautics and Space Administration Washington, D.C. 20546	

15. Supplementary Notes: The information presented is based on a portion of a thesis entitled "Studies in Tilt-Rotor VTOL Aircraft Aeroelasticity," submitted to Case Western Reserve University, Cleveland, Ohio, in partial fulfillment of requirements for the Ph.D. degree in Engineering Mechanics, June 1973.

16. Abstract

The manner of representing a flight vehicle structure as an assembly of beam, spring, and rigid-body components for vibration analysis is described. The development is couched in terms of a substructures methodology which is based on the finite-element stiffness method. The particular manner of employing beam, spring, and rigid-body components to model such items as wing structures, external stores, pylons supporting engines or external stores, and sprung masses associated with launch vehicle fuel slosh is described by means of several simple qualitative examples. A detailed numerical example consisting of a tilt-rotor VTOL aircraft is included to provide a unified illustration of the procedure for representing a structure as an equivalent system of beams, springs, and rigid bodies, the manner of forming the substructure mass and stiffness matrices, and the mechanics of writing the equations of constraint which enforce deflection compatibility at the junctions of the substructures. Since many structures, or selected components of structures, can be represented in this manner for vibration analysis, the modeling concepts described and their application in the numerical example shown should prove generally useful to the dynamicist.

17. Key Words (Suggested by Author(s))	18. Distribution Statement
Structural dynamics Vibration analysis Finite element beam modeling	Unclassified - Unlimited Subject Category 39

19. Security Classif. (of this report)	20. Security Classif. (of this page)	21. No. of Pages	22. Price*
Unclassified	Unclassified	100	$4.75

* For sale by the National Technical Information Service, Springfield, Virginia 22161

CONTENTS

CONSIDERATIONS FOR THE APPLICATION OF FINITE-ELEMENT BEAM MODELING TO VIBRATION ANALYSIS OF FLIGHT VEHICLE STRUCTURES*

Raymond G. Kvaternik
Langley Research Center

SUMMARY

The manner of representing a flight vehicle structure as an assembly of beam, spring, and rigid-body components for vibration analysis is described. The development is couched in terms of a substructures methodology which is based on the finite-element stiffness method. The particular manner of employing beam, spring, and rigid-body components to model such items as wing structures, external stores, pylons supporting engines or external stores, and sprung masses associated with launch vehicle fuel slosh is described by means of several simple qualitative examples. A detailed numerical example consisting of a tilt-rotor VTOL aircraft is included to provide a unified illustration of the procedure for representing a structure as an equivalent system of beams, springs, and rigid bodies, the manner of forming the substructure mass and stiffness matrices, and the mechanics of writing the equations of constraint which enforce deflection compatibility at the junctions of the substructures. Since many structures, or selected components of structures, can be represented in this manner for vibration analysis, the modeling concepts described and their application in the numerical example shown should prove generally useful to the dynamicist.

---

*The information presented herein is based on a portion of a thesis entitled "Studies in Tilt-Rotor VTOL Aircraft Aeroelasticity," which was submitted to Case Western Reserve University, Cleveland, Ohio, in partial fulfillment of the requirements for the degree of Doctor in Philosophy in Engineering Mechanics, June 1973.

INTRODUCTION

Customary engineering practice in dynamic analyses of complex aerospace structures consists of introducing some type of physical idealization to simplify the structure, establishing a finite-element mathematical model of the idealized system, and solving the resultant equations of motion. Finite-element models required for static analyses are usually quite complex in order to predict the stresses satisfactorily. For dynamic analyses, however, simpler models based on the use of (one-dimensional) beam elements to represent either the entire structure or selected components are often adequate (refs. 1 to 11).

A self-contained treatment of the practical aspects of applying finite-element beam modeling techniques in dynamic analyses is, for the most part, either lacking in the literature or of a fragmentary nature. The purpose of this report is to present a unified treatment of several aspects of finite-element beam modeling as might be applied to vibration analyses of flight vehicle structures. Herein, beam modeling is used in the general sense to include the use of beam, spring, and rigid-body components. The discussion is couched in terms of the substructures approach to vibration analysis as developed in reference 12. Several simple qualitative examples illustrating the manner of employing beams, springs, and rigid bodies to model such items as wing structures, external stores, pylons supporting engines or stores, and sprung masses associated with launch vehicle fuel slosh are given. A detailed numerical example consisting of a tilt-rotor VTOL aircraft structure is employed to illustrate the manner of representing a structure as an equivalent system of beam, spring, and rigid-body substructures, the formation of the substructure mass and stiffness matrices, and the mechanics of writing the equations of

constraint which enforce deflection compatibility at the junctions of the substructures. The direct method of vibration analysis as described in reference 12 and implemented in a special-purpose computer program designated SUDAN (SUbstructuring in Direct ANalyses) is used to solve for the modes and frequencies.

The present report relies on reference 12 for a complete understanding of the theoretical basis of the procedures implemented in the SUDAN program. For this reason it is recommended that reference 12 be used in conjunction with this report.

SYMBOLS

$[A],[B]$	submatrices of $[K]_B$
AE_i	extensional rigidity of ith beam element
$[C]$	submatrix of $[K]_B$; also matrix of coefficients of constraint equations expressed in discrete physical coordinates
e_i	offset of ith mass from beam elastic axis
EI_i	flexural rigidity of ith beam element
GJ_i	torsional rigidity of ith beam element
I_i	lumped torsional inertia at ith beam station
I_{ij}	components of rigid body inertia tensor (See eq. 15.)
$[\overline{K}]$	composite matrix containing free-body stiffness matrices of substructures as submatrices on the principal diagonal
$[K]_B$	stiffness matrix for beam bending
$[K]_{B-S}$	stiffness matrix for beam-spring
$[K]_T$	stiffness matrix for beam torsion
$[\Delta K]$	matrix of additional spring stiffness terms
$[K]_E$	stiffness matrix for beam extension
$[\overline{\mathcal{K}}]$	composite matrix containing the free-body modal stiffness matrices of substructures as submatrices on the principal diagonal
$[k]^{(i)}$	stiffness matrix of ith substructure regarded as a free-body
K_{a_1}, K_{b_1}	longitudinal and lateral hub flapping spring rates
L_i	lengths; length of ith beam element
M	mass of rigid body component
$[\overline{M}]$	composite matrix containing free-body mass matrices of substructures as submatrices on the principal diagonal

m_i, M_i	lumped mass at ith beam station
$[M]_B$	mass matrix for beam bending
$[M]_T$	mass matrix for beam torsion
$[M]_E$	mass matrix for beam extension
$[\bar{\mathcal{M}}]$	composite matrix containing the free-body modal mass matrices of substructures as submatrices on the principal diagonal
$[M]_{B+RB}$	beam + rigid body mass matrix
$[M]_{B+T}$	coupled bending-torsion mass matrix
$[M]_{C-T}$	mass matrix of wing carry-through structure
$[M]_{ROTOR}$	mass matrix of rotor
$[M]_{PYLON}$	mass matrix of pylon
$[M]_{RB}$	mass matrix of rigid body
$[m]^{(i)}$	mass matrix of ith substructure regarded as a free body
$\{p\}^{(i)}$	column matrix of discrete, physical coordinates for ith substructure regarded as a free body
q	generalized coordinate
q_j	jth nodal degree of freedom
$\{q\}, \{z\}$	column matrix containing the discrete, physical coordinates of all the substructures
$[R], [T], [L]$	connection coordinate transformation matrices
RI_i	lumped rotary inertia at ith beam station
RI	rotary inertia of rigid body about its center of gravity
T	kinetic energy

T_i	kinetic energy of ith wing section
[U]	uncoupled system modal expansion matrix containing substructure modal subsets on principal diagonal
u	extensional displacement of beam
u_i	extensional displacement of beam at ith station
V	potential energy
w	bending displacement of beam
w_i	bending displacement of beam at ith station
$\{X\}_r$	column vector of junction coordinates, r = 1, 2, . . ., 15
$\{X\}^s$	column vector of auxiliary coordinates, s = i, ii, . . ., vii
x,y,z	displacements
x_r, y_r, z_r	connection coordinate displacements
α, β, γ	rotations
$\alpha_r, \beta_r, \gamma_r$	connection coordinate rotations
$\{X\}_r$	proprotor disc coordinate vector
θ	bending slope of beam
θ_c	pylon tilt angle forward from vertical position
θ_i	angles; bending slope of beam at ith station
$\{\xi\}$	column matrix containing all substructure modal coordinates
ϕ_i	twist of beam at ith station

Physical quantities in this report are given in the International System of Units (SI). The calculations were made in Customary Units.

SUBSTRUCTURES APPROACH TO DYNAMIC ANALYSIS

Three distinct steps may be identified with dynamic analyses based on a substructures approach: partitioning into substructures, discretization of the substructures, and assembly of the mathematical models of the substructures. Structural partitioning consists of dividing the structure into a collection of smaller components or substructures which can be more easily handled. An illustration of such a partitioning is depicted in Figure 1. Discretization involves establishing a finite-element mathematical model of each isolated substructure based on the known inertial and elastic properties of the substructures. Detailed considerations relating to finite-element modeling are available in several books. (See, for example, references 13 to 17.) Application of the finite-element stiffness matrix method to each substructure regarded as a free body leads to a discrete mass matrix $[m]$, a discrete stiffness matrix $[k]$, and a vector of discrete coordinates* $\{p\}$ for each substructure. The free vibration equations of motion corresponding to each substructure can be collected into one partitioned diagonal matrix equation having the uncoupled form

$$\begin{bmatrix} [m]^{(1)} & & & \\ & [m]^{(2)} & & \\ & & \ddots & \\ & & & [m]^{(NS)} \end{bmatrix} \begin{Bmatrix} \{\ddot{p}\}^{1} \\ \{\ddot{p}\}^{2} \\ \vdots \\ \{\ddot{p}\}^{(NS)} \end{Bmatrix} + \begin{bmatrix} [k]^{(1)} & & & \\ & [k]^{(2)} & & \\ & & \ddots & \\ & & & [k]^{(NS)} \end{bmatrix} \begin{Bmatrix} \{p\}^{(1)} \\ \{p\}^{(2)} \\ \vdots \\ \{p\}^{(NS)} \end{Bmatrix} = \begin{Bmatrix} \{0\}^{(1)} \\ \{0\}^{(2)} \\ \vdots \\ \{0\}^{(NS)} \end{Bmatrix} \tag{1}$$

*Discrete coordinates define the translations and rotations at a set of discrete points.

where NS is equal to the number of substructures into which the structure has been divided. For notational convenience equation 1 is written in the compact form

$$[\overline{M}]\ \{\ddot{z}\} + [\overline{K}]\ \{z\} = \{0\} \tag{2}$$

For the substructures shown in Figure 1, for example, the composite matrices $[\overline{M}]$ and $[\overline{K}]$ appearing in equation 2 each would have the form given diagrammatically in Figure 2. Each block in Figure 2 represents the mass or stiffness matrix appropriate to a substructure. The ordering of the submatrices within $[\overline{M}]$ and $[\overline{K}]$, though required to be consistent, is arbitrary. For component mode synthesis the modal equivalent of equation 2 is

$$[\overline{\mathcal{M}}]\ \{\ddot{\xi}\} + [\overline{\mathcal{K}}]\ \{\xi\} = \{0\} \tag{3}$$

where $[\overline{\mathcal{M}}]$ and $[\overline{\mathcal{K}}]$ are the composite matrices containing the substructure modal mass and stiffness matrices as submatrices on the principal diagonal.

A consequence of any substructuring procedure is the introduction of coordinates which are not generalized coordinates but are related by equations of constraint which must be imposed to restore geometric compatibility at the interfaces of the substructures. Since the matrices $[\overline{M}]$ and $[\overline{K}]$ in equation 2 and $[\overline{\mathcal{M}}]$ and $[\overline{\mathcal{K}}]$ in equation 3 are established on the basis of such a substructuring procedure, neither the coordinates forming the vector $\{z\}$ nor those forming the vector $\{\xi\}$ are independent. The dependency equations relating the various discrete coordinates in $\{z\}$ can be put into the matrix form

$$[C]\ \{z\} = \{0\} \tag{4}$$

and those relating the various modal coordinates in $\{\xi\}$ can be put into the form

$$[C]\,[U]\,\{\xi\} = \{0\} \tag{5}$$

where $[C]$ is a constant matrix depending solely on the geometric configuration of the interfaces and $[U]$ is the uncoupled system modal expansion matrix. A set of independent coordinates consistent with the appropriate equations of constraint must be established. Usual practice when dealing with equations of constraint (see ref. 18, for example) is to select certain of the coordinates as independent coordinates and express the remaining dependent coordinates in terms of those which have been selected to be independent by solving the constraint equations as simultaneous equations. A different approach to establishing independent coordinates in the presence of equations of constraint is an algorithm (ref. 19) which is based on solving an eigenvalue problem associated with a symmetric matrix formed from the coefficients of the constraint equations. The basis of these procedures is summarized in reference 12.

BEAM MODELING OF SUBSTRUCTURES

General Considerations

Since the substructures are treated as distinct and separate components in a substructuring methodology, their structural properties are most conveniently defined relative to axes local to each component. The specification of the mass and stiffness matrices corresponding to each of the three types of structural members employed in the beam modeling of a structure is the subject of the following subsections.

Substructures treated as beams.- The elastic properties of substructures treated as beams are taken to be defined in terms of the distribution of flexural, torsional, and extensional stiffness (EI, GJ, and AE, respectively) along a theoretically defined elastic axis. The continuous distortion of the beam in extension, torsion, and bending in two perpendicular planes is approximated by specifying appropriate deflections and rotations at a number of discrete points or stations along the elastic axis of the beam. A beam segment or element is defined to be the length between two such stations. The stiffness of each element is assumed to be constant and given by the average value of the stiffnesses at the two adjacent stations. The distributed mass of the beam is discretized by replacing the distributed mass within mean locations on either side of the stations established by statically equivalent concentrated masses at each of the stations along the beam. In general, each mass has three components of translational inertia and three components of rotational inertia. Mass static unbalance about the local elastic axis is also preserved.

The mass and stiffness matrices of an unrestrained, arbitrarily oriented beam element are each of order 12 × 12, three translational and three rotational degrees of freedom being associated with each of its two ends. If the local coordinate axes are chosen to coincide with the principal axes of the cross section, the 12 × 12 stiffness matrix can be expressed in terms of uncoupled 4 × 4 and 2 × 2 submatrices located on the principal diagonal (ref. 13). A similar partitioning is possible for the mass matrix if the centers of gravity of the sectional masses are located on the elastic axis of the beam. In general, however, the sectional centers of gravity of the original component will not lie along its elastic axis. This will lead to additional, off-diagonal, mass terms which will couple bending and torsion and/or bending and extensional motion.

It will be assumed that the sectional centers of gravity lie on the elastic axis for the present and later in the report it will be shown how to account for any mass coupling terms. The form of these submatrices for a beam substructure is shown below for the two-element beam shown in figure 3.

Beam bending.- The stiffness matrix for vertical bending is put into the partitioned form:

$$[K]_B = \begin{array}{c} \begin{array}{cc} w & \theta \end{array} \\ \left[\begin{array}{c|c} [A] & [B] \\ \hline [B]^T & [C] \end{array}\right] \end{array} \begin{array}{c} \\ \left[\begin{array}{c} w \\ \hline \theta \end{array}\right] \end{array} \tag{6}$$

where, for a beam modeled using two elements,

$$[A] = \begin{array}{c} \begin{array}{ccc} w_1 & w_2 & w_3 \end{array} \\ \begin{bmatrix} \frac{12EI_1}{L_1^3} & -\frac{12EI_1}{L_1^3} & 0 \\ -\frac{12EI_1}{L_1^3} & \frac{12EI_1}{L_1^3} + \frac{12EI_2}{L_2^3} & -\frac{12EI_2}{L_2^3} \\ 0 & -\frac{12EI_2}{L_2^3} & \frac{12EI_2}{L_2^3} \end{bmatrix} \end{array} \begin{array}{c} \\ \begin{bmatrix} w_1 \\ w_2 \\ w_3 \end{bmatrix} \end{array} \tag{7}$$

$$[B] = \begin{array}{c} \begin{array}{ccc} \theta_1 & \theta_2 & \theta_3 \end{array} \\ \begin{bmatrix} \frac{6EI_1}{L_1^2} & \frac{6EI_1}{L_1^2} & 0 \\ -\frac{6EI_1}{L_1^2} & -\frac{6EI_1}{L_1^2}+\frac{6EI_2}{L_2^2} & \frac{6EI_2}{L_2^2} \\ 0 & -\frac{6EI_2}{L_2^2} & -\frac{6EI_2}{L_2^2} \end{bmatrix} \end{array} \begin{bmatrix} w_1 \\ w_2 \\ w_3 \end{bmatrix} \qquad (8)$$

$$[C] = \begin{array}{c} \begin{array}{ccc} \theta_1 & \theta_2 & \theta_3 \end{array} \\ \begin{bmatrix} \frac{4EI_1}{L_1} & \frac{2EI_1}{L_1} & 0 \\ \frac{2EI_1}{L_1} & \frac{4EI_1}{L_1}+\frac{4EI_2}{L_2} & \frac{2EI_2}{L_2} \\ 0 & \frac{2EI_2}{L_2} & \frac{4EI_2}{L_2} \end{bmatrix} \end{array} \begin{bmatrix} \theta_1 \\ \theta_2 \\ \theta_3 \end{bmatrix} \qquad (9)$$

The bending displacements and slopes have each been grouped together and placed in the order shown in equation 6 for convenience in their computer implementation. Extension to additional elements is apparent in the distinctive forms of [A], [B], and [C]. The corresponding inertia matrix is given by

$$[M]_B = \begin{array}{c|ccc|ccc} & w_1 & w_2 & w_3 & \theta_1 & \theta_2 & \theta_3 \\ \hline w_1 & M_1 & & & & & \\ w_2 & & M_2 & & & & \\ w_3 & & & M_3 & & & \\ \hline \theta_1 & & & & RI_1 & & \\ \theta_2 & & & & & RI_2 & \\ \theta_3 & & & & & & RI_3 \end{array} \qquad (10)$$

where the matrix elements not shown are zero. Similar matrix expressions describe lateral bending.

Beam torsion: The torsional stiffness matrix is given by

$$[K]_T = \begin{array}{c|ccc} & \phi_1 & \phi_2 & \phi_3 \\ \hline \phi_1 & \frac{GJ_1}{L_1} & -\frac{GJ_1}{L_1} & 0 \\ \phi_2 & -\frac{GJ_1}{L_1} & \frac{GJ_1}{L_1}+\frac{GJ_2}{L_2} & -\frac{GJ_2}{L_2} \\ \phi_3 & 0 & -\frac{GJ_2}{L_2} & \frac{GJ_2}{L_2} \end{array} \qquad (11)$$

and the torsional inertia matrix by

$$[M]_T = \begin{array}{c} \begin{bmatrix} \phi_1 & \phi_2 & \phi_3 \end{bmatrix} \\ \begin{bmatrix} I_1 & & \\ & I_2 & \\ & & I_3 \end{bmatrix} \\ \begin{bmatrix} \phi_1 \\ \phi_2 \\ \phi_3 \end{bmatrix} \end{array} \tag{12}$$

Extension to more elements is obvious.

Beam extension: The stiffness matrix describing extensional (axial) deformation has the form

$$[K]_E = \begin{array}{c} \begin{bmatrix} u_1 & u_2 & u_3 \end{bmatrix} \\ \begin{bmatrix} \frac{AE_1}{L_1} & -\frac{AE_1}{L_1} & 0 \\ -\frac{AE_1}{L_1} & \frac{AE_1}{L_1}+\frac{AE_2}{L_2} & -\frac{AE_2}{L_2} \\ 0 & -\frac{AE_2}{L_2} & \frac{AE_2}{L_2} \end{bmatrix} \\ \begin{bmatrix} u_1 \\ u_2 \\ u_3 \end{bmatrix} \end{array} \tag{13}$$

and the corresponding inertia matrix is

$$[M]_E = \begin{array}{c} \begin{bmatrix} u_1 & u_2 & u_3 \end{bmatrix} \\ \begin{bmatrix} M_1 & & \\ & M_2 & \\ & & M_3 \end{bmatrix} \\ \begin{bmatrix} u_1 \\ u_2 \\ u_3 \end{bmatrix} \end{array} \tag{14}$$

Again, the extension to additional elements is obvious.

Substructures treated as springs.- In many instances actual springs may comprise some of the components of a structure or members may be treated as one- or two-degree-of-freedom springs depending on whether they have one end tied to ground or both ends free. These springs are defined by 1×1 or 2×2 stiffness matrices having spring constants as matrix elements and associated 1×1 or 2×2 inertia matrices which are null (zero).

When modeling short structural components as beams it is sometimes convenient to account for their elastic characteristics in the definition of the substructure but to include their inertial properties with adjacent components. A massless, uniform beam segment is employed for this purpose. Since only the elastic properties of this beam segment are considered it has the character of a spring and it seems appropriate to include its description here. For descriptive purposes this massless beam segment will be referred to as a "beam-spring" herein. The 12×12 stiffness matrix for the beam-spring having the coordinate ordering shown in figure 4 has the form given in figure 5. The corresponding inertia matrix is taken to be null.

Substructures treated as rigid bodies.- Components such as ordnance, external fuel tanks, engine/nacelle combinations, etc., can often be treated as rigid in dynamic analyses. The inertia matrices of such rigid bodies with respect to local body axes at the center of gravity have the general form

$$[M]_{RB} = \begin{array}{c} \begin{array}{cccccc} x & y & z & \alpha & \beta & \gamma \end{array} \\ \left[\begin{array}{ccc:ccc} M & & & & & \\ & M & & & & \\ & & M & & & \\ \hdashline & & & I_{xx} & I_{xy} & I_{xz} \\ & & & I_{yx} & I_{yy} & I_{yz} \\ & & & I_{zx} & I_{zy} & I_{zz} \end{array}\right] \end{array} \begin{array}{c} x \\ y \\ z \\ \alpha \\ \beta \\ \gamma \end{array} \qquad (15)$$

where the elements not shown are zero. The corresponding stiffness matrices are null since a rigid body has no strain energy associated with its motion.

Oftentimes, while it may be necessary to account for the translational or rotational rigid-body motion of a beam substructure in some direction, the corresponding deformation can be neglected. This situation is easily accommodated by this rigid-body component.

Once the mass and stiffness matrices for the substructures have been determined, the mass and stiffness matrices for the complete structure are given by the composite matrices formed by locating the substructure matrices along the principal diagonal. These composite matrices are denoted $[\overline{M}]$ and $[\overline{K}]$, respectively. For the "stick" model shown in figure 6, for example, $[\overline{M}]$ and $[\overline{K}]$ would have the form shown in figure 7. It should be noted that the stick model of figure 6 and the particular freedoms indicated in figure 7 are appropriate to a symmetric vibration analysis. Each block in figure 7 corresponds to a submatrix. The ordering of these submatrices within the larger substructure submatrices (indicated by braces) and the ordering of substructure submatrices

within $[\bar{M}]$ and $[\bar{K}]$ must be compatible but is otherwise arbitrary. Since the mass and stiffness matrices for each substructure are generated independently, no inter-substructure coupling exists in $[\bar{M}]$ or $[\bar{K}]$. However, intra-substructure coupling (i.e., coupling between submatrices within a substructure submatrix through off-diagonal terms) can exist. Situations in which such coupling arises will now be discussed.

Specific Considerations

If the sectional centers of gravity of the lumped masses for the beam substructures do not fall on the elastic axis, there will arise mass static unbalance terms which will couple two or more of the blocks in the mass matrix for the beam substructure. For example, if the sectional centers of gravity of the wing or tail surfaces of the airplane in figure 6 were displaced from their elastic axes in the plane of the surface the mass static unbalance terms would appear outside the block diagonal areas indicated in figure 7 and couple the vertical bending and torsion submatrices in the matrices for the wing or tail substructures in $[\bar{M}]$. Mass coupling terms of this type will also occur if a rigid body component is not treated as a unique substructure (as discussed earlier) but has its mass matrix combined with the mass matrix of the beam component to which it is attached. If, for example, the main landing gear assembly of the aircraft shown in figure 6 were treated as a rigid mass and its inertial properties combined with the forward fuselage beam, the vertical bending and axial rigid body submatrices of the forward fuselage beam substructure in $[\bar{M}]$ would be coupled.* Coupling terms would also arise <u>within</u> the vertical

*For an anti-symmetric analysis the lateral bending and torsion blocks of the substructure would be coupled.

bending block, leading to a non-diagonal mass matrix for beam bending. Inter- and intra-substructure coupling terms arise in the stiffness matrix of the partitioned structure, $[\overline{K}]$, when the stiffness characteristics of springs which are not treated as substructures are combined with the stiffness matrices of members to which they are attached rather than treated as separate substructures. These aspects, as well as others, are elucidated below in several simple qualitative examples.

Treatment of mass static unbalance.- Consider the sectionalized wing planform shown in figure 8. The section (lumped) masses, bending inertias, and torsional inertias (about the c.g.) are denoted by M_i, RI_i, and I_i, respectively. The perpendicular distance between the section c.g. locations (assumed to be in the wing chord plane) and the wing elastic axis are denoted by e_i. The kinetic energy of each section, T_i, expressed in terms of displacements and rotations of the elastic axis station, has the form indicated at the bottom of figure 8. Substituting this expression into Lagrange's equation

$$\frac{d}{dt}\left(\frac{\partial T}{\partial \dot{q}}\right) - \frac{\partial V}{\partial q} = 0 \tag{16}$$

and performing the appropriate differentiations leads to the coupled bending-torsion mass matrix shown in figure 9. Assuming figure 8 is appropriate to the wing of the aircraft in figure 6, then $[\overline{M}]$ has the form shown in figure 7. The first two blocks of substructure #4 would be given by twice the mass matrix of figure 9. If the sectional center of gravities were also displaced vertically from the wing elastic axis (i.e., not in the wing chord plane) additional coupling terms would arise and the vertical bending, torsion, and fore-and-aft bending blocks of substructure #4 would be coupled.

Alternative treatment of rigid bodies.- As an alternative to treating a rigid body as a substructure, the inertial properties of the rigid body (total mass lumped at the c.g. and moments and products of inertia relative to axes fixed in the body at the c.g.) can be combined with the inertia matrix of the elastic component to which it is attached. This treatment has the advantage of not explicitly introducing the degrees of freedom associated with the rigid body into the problem.

Rigid attachment: If the rigid body is rigidly attached to an elastic substructure, the procedure consists in modifying the kinetic energy expression for the substructure to include the effects of the concentrated mass, inertia, and static unbalance about its point of attachment. For example, consider the situation depicted in figure 10. Suppose one wishes to combine the inertial properties of the center-line fuel tank, regarded as a rigid body, with the inertia matrix of the fuselage beam by regarding the tank as rigidly connected to the nth fuselage beam station. Assume that each fuselage mass has both vertical bending and longitudinal degrees of freedom. If the principal inertia axes of the fuel tank are parallel to the principal geometric axes of the fuselage beam the kinetic energy of the tank expressed in terms of the motion at the nth mass station on the beam has the form given at the bottom of figure 10. Substituting this expression into Lagrange's equation gives the matrix of additional terms which must be added to the mass matrix (assumed to be diagonal) for the fuselage beam. The final mass matrix is given in figure 11.

Flexible attachment: If the fuel tank of figure 10 were attached to the fuselage beam through a flexible member which could be treated as a spring substructure the inertia properties of the tank could be combined with the (null)

inertia matrix of the spring substructure using a procedure similar to that described directly above.

Alternative treatment of springs.- For convenience, springs can be divided into those which have one end tied to ground (one-degree-of-freedom springs) and those which have both ends "free" (two-degree-of-freedom springs) in the sense that while both ends are attached to some component, neither end is tied to ground.

Springs having one end tied to ground: If the spring attachment point on the structure is on the elastic axis at a point identified as a degree of freedom, the spring constant(s) can be simply added to the appropriate diagonal term(s) of the stiffness matrix of the component. If the point of attachment is on the elastic axis but not at a point identified as a degree of freedom, coupling will occur. In the latter case it is sometimes convenient to introduce an auxiliary massless station at the spring attachment point. Similar considerations apply to the case where the spring is connected to the elastic axis through a rigid offset. These situations are depicted in figure 12a. The general form of the additional stiffness terms due to springs attached to the elastic axis at a station identified as a degree of freedom is indicated in figure 13a.

Free-free springs: The spring constants of springs which have neither end tied to ground, such as given in figure 12b, can be combined with the stiffness matrices of the substructures to which they are attached by writing the potential energy of the springs in terms of coordinates at the points of attachment. The general form of the additional stiffness terms due to the spring coupling of figure 12b is shown in figure 13b. A specific illustration of the use of this expedient in the realm of launch vehicle dynamics may be given with the aid of figure 14.

In dynamic analyses of launch vehicles the dynamic effects of sloshing propellants are usually included by introducing a dynamically equivalent mechanical analogy, composed of fixed and oscillating masses connected to the tank by springs or pendulums, to account for each important vibration mode of the liquid as a degree of freedom (ref. 20). This equivalent lumped-parameter mathematical model can then be combined with appropriate discrete-element representations for other components of the vehicle. A spring-mass analogy is shown in figure 14. One such spring-mass assembly is provided to represent the dynamic effects of sloshing accompanying vertical bending (translation and rotation) and longitudinal oscillation. For illustrative simplicity, all three sloshing masses are taken to be attached to the same (nth) beam station. The non-sloshing portion of the fluid would simply be combined with the beam mass at the nth station of the beam. The potential energy of the springs, expressed in terms of the deflections of the nth beam station $\left(w_n,\ \theta_n,\ u_n\right)$ and the deflections of the slosh masses $(w,\ \theta,\ u)$, is given by V in the figure. Substituting this expression into Lagrange's equation leads to the matrix $[\Delta K]$ shown in figure 15. $[\Delta K]$ is the matrix of spring stiffness terms which must be added to the stiffness matrix for the beam.

ILLUSTRATIVE EXAMPLE

An example illustrating the manner of modeling an aircraft structure using beam, spring, and rigid body components, the manner of forming the substructure mass and stiffness matrices, and the mechanics of writing the equations of constraint for a structural configuration of some engineering complexity is presented in this section. The subject configuration is the tilt-rotor VTOL aircraft design shown in figure 16. It should be emphasized that the

idealization of a complete aircraft as a simple "stick" model using a beam-type representation for all the structural components should be applied with engineering judgement. Such a simplification may be inadequate to account for the influence of such things as large structural cutouts in the airframe (e.g., doorways) and highly redundant structural components (e.g., wing carry-through box). The intent of the following example is solely to provide an illustration of the practical aspects of the application of beam modeling which can be readily adapted to other configurations.

Beam Model Representation of Aircraft

The subject aircraft is depicted in silhouette form in figure 17 along with the idealized model established using the beam, spring, and rigid-body components described above. The fuselage, wing, and empennage structures are replaced by non-uniform beams lying along the theoretical elastic axes of the respective components. Since the fuselage elastic axis has two changes in slope, three beams are used to represent the fuselage structure. The root ends of the wing and vertical tail beams are located at the periphery of fuselage cross-section. The wing carry-through structure joining the root ends of the wings is idealized as a beam-spring, its (rigid-body) inertial properties being combined with the inertia matrix of the second fuselage beam. The geometric offset between the second fuselage beam and the wing carry-through beam-spring represents the fuselage depth between the fuselage elastic axis and the carry-through elastic axis. The transition from the fuselage beam to the wing carry-through beam is made by equations of constraint to express a rigid connection. A similar treatment is employed for the geometric offset between the aft fuselage beam and the vertical tail beam. The pylon structure, consisting of the

transmission/engine assembly, is treated as a rigid body while the mast (the portion of the drive shaft extending forward from the transmission) on which each proprotor is mounted is treated as a beam-spring. The geometric offset between the wing elastic axis at the wing tip and the position on the transmission centerline through which the conversion axis about which the pylon tilts passes is specified to be rigid via equations of constraint. The proprotor blades are assumed to be rigid. Since the blades are rigidly attached to the hub in a gimbaled proprotor design (such as the design depicted in fig. 16) the proprotors (assumed to be non-rotating) are treated as rigid discs in the analysis. The hub is initially taken to be rigidly attached to the mast. However, for illustrative purposes, the manner of treating a hub which is spring-connected to the mast will also be described.

Since the substructures are treated as independent components, their structural properties and deflection characteristics are most conveniently defined relative to axes local to each component. The existence of such local axes for the definition of these quantities is assumed herein. The local component axis systems are also employed to establish the deflection compatibility equations at the junctions of the substructures. The set of right-handed local junction coordinate axes used in writing the equations of constraint is identifiable by subscripts in figure 18. Each of the directions so indicated is taken to be positive. Vectors representing positive rotations α_r, β_r, γ_r (not shown) about x_r, y_r, z_r, respectively, are taken in the same direction as vectors representing positive x_r, y_r, z_r. A shorthand notation for a column vector of these junction, or connection, coordinates is given by $\{X\}_r$ where

$$\{X\}_r = \begin{Bmatrix} x_r \\ y_r \\ z_r \\ \alpha_r \\ \beta_r \\ \gamma_r \end{Bmatrix} \equiv \begin{Bmatrix} x \\ y \\ z \\ \alpha \\ \beta \\ \gamma \end{Bmatrix}_r \qquad (17)$$

$$r = 1,2,\ldots,15$$

Several auxiliary right-handed coordinate systems (which are not associated with degrees of freedom) are employed to facilitate writing the constraint equations. These auxiliary coordinate systems are also shown in figure 18 and are distinguished by Roman numeral superscripts. A shorthand notation for a column vector of these auxiliary coordinates is given by $\{X\}^s$ where

$$\{X\}^s \equiv \begin{Bmatrix} x^s \\ y^s \\ z^s \\ \alpha^s \\ \beta^s \\ \gamma^s \end{Bmatrix} \equiv \begin{Bmatrix} x \\ y \\ z \\ \alpha \\ \beta \\ \gamma \end{Bmatrix}^s \qquad (18)$$

$$s = i,ii,\ldots,vii$$

The structural data for the fuselage, wing, and empennage of this design were available (ref. 21) in the form of bar graphs showing the distribution of mass, rotary inertia, and mass static unbalance and curves showing the variation of EI and GJ along the calculated elastic axis of each member. The wing and

tail inertial data were based on cuts perpendicular to the elastic axis. Data for the proprotor and pylon consisted of lumped mass properties and selected EI/GJ characteristics. Employing these data, lumped-mass/stiffness discretizations were established for the fuselage, wing, and empennage beams. These are summarized in Tables 1 to 3. Inertial properties of components treated as rigid bodies and beam-springs are given in Table 4 while the elastic properties of beam-spring components are listed in Table 5. A summary of the pertinent geometric quantities is contained in Table 6. Utilizing aircraft symmetry about a vertical plane through the center of the fuselage, explicit consideration need be given to only one-half of the aircraft. A consequence of this separate treatment of the symmetric and anti-symmetric problems is the identification of displacements and rotations in each formulation which can be set to zero. It is convenient to distinguish the coordinates constituting the vectors $\{X\}_r$ from the actual nodal degrees of freedom. The nodal degrees of freedom are denoted by q_j herein. The column vector containing all these freedoms, $\{q\}$, may be directly identified with the vector $\{z\}$ in equations 2 and 4.

Symmetric Formulation

For the symmetric analysis the airframe motions considered are pitch bending of the fuselage, bending and torsion of the wing and horizontal tail, and fore and aft bending of the vertical tail. The aircraft was divided into 10 substructures having a total of 144 degrees of freedom. The substructures employed and the corresponding degrees of freedom are identified in figure 19 and Table 7, respectively.

Constraint equations.- Connection of the various substructures is achieved through the use of equations of constraint which mathematically enforce

deflection compatibility at the interfaces of the substructures. The deflection vectors of adjacent substructures at their point of attachment must be equal when expressed in a common local coordinate system. The common systems considered here are coincident with the local coordinate systems of the contiguous substructures. The deflection vectors of adjacent substructures at their point of attachment are related by a diagonally partitioned rotational transformation matrix [R]. Since small rotations can be treated as vectors the rotations at attachment points are related by the same matrix as the displacements. The two submatrices comprising [R] are thus identical and are denoted by [T]. For the general three-dimensional problem with six degrees of freedom associated with each station, [T] is of order 3×3 and [R] is of order 6×6.

In the remainder of this section figure 18 will be used in conjunction with auxiliary sketches, interspersed throughout the text, showing the substructure junctions and associated coordinate systems in order to aid in writing the equations of constraint.

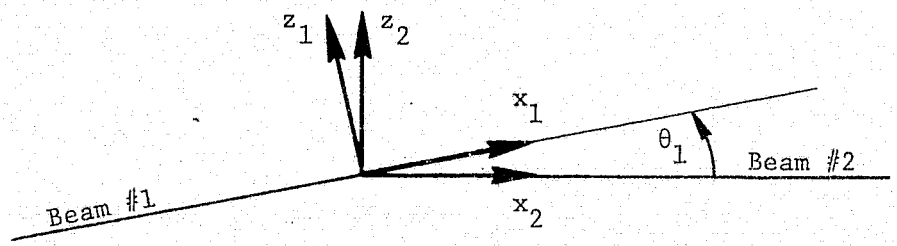

Sketch 1.- Junction of fuselage beam #1 and fuselage beam #2.

The expression relating the equality of the deflections at the left end of beam #2 and the right end of beam #1 relative to coordinates local to beam #2 has the form

$$\begin{Bmatrix} x \\ y \\ z \\ \alpha \\ \beta \\ \gamma \end{Bmatrix}_2 = \left[\begin{array}{c|c} [T_1] & [0] \\ \hline [0] & [T_1] \end{array}\right] \begin{Bmatrix} x \\ y \\ z \\ \alpha \\ \beta \\ \gamma \end{Bmatrix}_1 \equiv [R_1]\{X\}_1 \tag{19}$$

where the vectors $\{X\}_1$ and $\{X\}_2$ are identified with degrees of freedom according to

$$\begin{Bmatrix} x \\ y \\ z \\ \alpha \\ \beta \\ \gamma \end{Bmatrix}_2 = \begin{Bmatrix} q_{24} \\ 0 \\ q_{12} \\ 0 \\ -q_{18} \\ 0 \end{Bmatrix} \qquad \begin{Bmatrix} x \\ y \\ z \\ \alpha \\ \beta \\ \gamma \end{Bmatrix}_1 = \begin{Bmatrix} q_{11} \\ 0 \\ q_5 \\ 0 \\ -q_{10} \\ 0 \end{Bmatrix} \tag{20}$$

and the coordinate rotation matrix $[T_1]$ is given by

$$[T_1] \equiv \begin{bmatrix} \cos\theta_1 & 0 & -\sin\theta_1 \\ 0 & 1 & 0 \\ \sin\theta_1 & 0 & \cos\theta_1 \end{bmatrix} \tag{21}$$

Since there are no displacements or rotations out of the vertical plane of symmetry in a symmetric formulation y_1, α_1, γ_1, y_2, α_2, and γ_2 are zero. The negative signs associated with q_{18} and q_{10} in equations 20 have been introduced in order to have the usual definition of positive slope. This has been done here merely for convenience. Several sign changes of this type will be introduced during the course of this development for similar reasons. Expanding equation 19 using equations 20 and 21, the resultant constraint equations at this junction are given by

$$\begin{aligned} q_{24} &= q_{11} \cos \theta_1 - q_5 \sin \theta_1 \\ q_{12} &= q_{11} \sin \theta_1 + q_5 \cos \theta_1 \\ -q_{18} &= -q_{10} \end{aligned} \tag{22}$$

For brevity, the remaining constraint equations to be developed will not be written out piecemeal in the expanded form analogous to equation 22. A summary of all the constraint equations in expanded form will be given in an appendix.

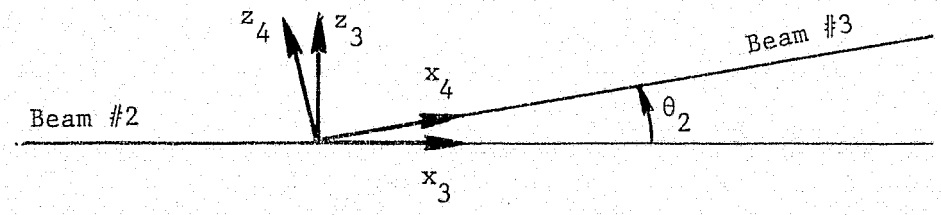

Sketch 2.- Junction of fuselage beam #2 and fuselage beam #3.

At the junction of fuselage beams #2 and #3

$$\begin{Bmatrix} x \\ y \\ z \\ \alpha \\ \beta \\ \gamma \end{Bmatrix}_3 = \left[\begin{array}{c|c} [T_2] & [0] \\ \hline [0] & [T_2] \end{array}\right] \begin{Bmatrix} x \\ y \\ z \\ \alpha \\ \beta \\ \gamma \end{Bmatrix}_4 \tag{23}$$

where

$$\begin{Bmatrix} x \\ y \\ z \\ \alpha \\ \beta \\ \gamma \end{Bmatrix}_3 = \begin{Bmatrix} q_{24} \\ 0 \\ q_{17} \\ 0 \\ -q_{23} \\ 0 \end{Bmatrix} \qquad \begin{Bmatrix} x \\ y \\ z \\ \alpha \\ \beta \\ \gamma \end{Bmatrix}_4 = \begin{Bmatrix} q_{41} \\ 0 \\ q_{25} \\ 0 \\ -q_{33} \\ 0 \end{Bmatrix} \tag{24}$$

and

$$[T_2] = \begin{bmatrix} \cos\theta_2 & 0 & -\sin\theta_2 \\ 0 & 1 & 0 \\ \sin\theta_2 & 0 & \cos\theta_2 \end{bmatrix} \tag{25}$$

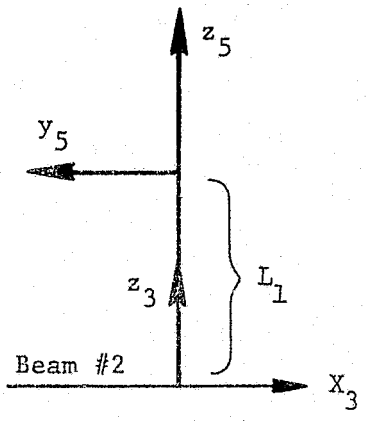

Sketch 3.- Geometric offset between fuselage and wing carry-through.

A rigid link is used to model the geometric offset between fuselage beam #2 and the wing carry-through beam-spring. The equations relating the deflections at the aft end of fuselage beam #2 to the deflections of the inboard end of the wing carry-through beam-spring are then

$$\begin{Bmatrix} x \\ y \\ z \\ \alpha \\ \beta \\ \gamma \end{Bmatrix}_3 = \left[\begin{array}{ccc|ccc} 0 & -1 & 0 & -L_1 & 0 & 0 \\ 1 & 0 & 0 & 0 & -L_1 & 0 \\ 0 & 0 & 1 & 0 & 0 & 0 \\ \hline 0 & 0 & 0 & 0 & -1 & 0 \\ 0 & 0 & 0 & 1 & 0 & 0 \\ 0 & 0 & 0 & 0 & 0 & 1 \end{array}\right] \begin{Bmatrix} x \\ y \\ z \\ \alpha \\ \beta \\ \gamma \end{Bmatrix}_5 \tag{26}$$

where

$$\begin{Bmatrix} x \\ y \\ z \\ \alpha \\ \beta \\ \gamma \end{Bmatrix}_5 = \begin{Bmatrix} 0 \\ q_{42} \\ q_{43} \\ q_{44} \\ q_{45} \\ q_{46} \end{Bmatrix} \tag{27}$$

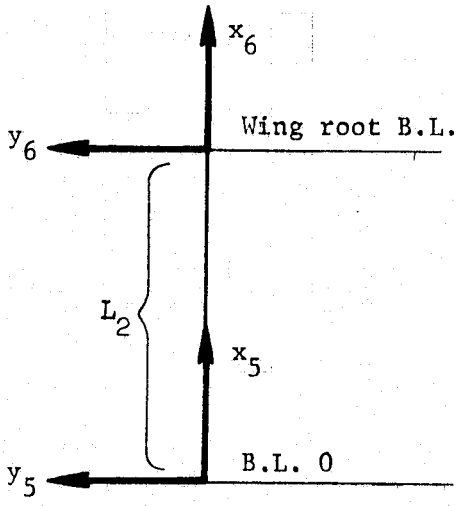

$$\begin{Bmatrix} x \\ y \\ z \\ \alpha \\ \beta \\ \gamma \end{Bmatrix}_6 = \begin{Bmatrix} q_{47} \\ q_{48} \\ q_{49} \\ q_{50} \\ q_{51} \\ q_{52} \end{Bmatrix} \tag{28}$$

Sketch 4.- Wing carry-through structure.

Twisting of the wing carry-through structure was judged to be negligible in a symmetric mode of oscillation. Hence, the wing carry-through structure is taken to be rigid. This condition may be specified by the constraint

$$q_{50} - q_{44} = 0 \tag{29}$$

Extensional deformations of this member are also assumed to be negligible. Since $x_5 = 0$ (cf. eq. 27) this implies the additional constraint

$$q_{47} = 0 \tag{30}$$

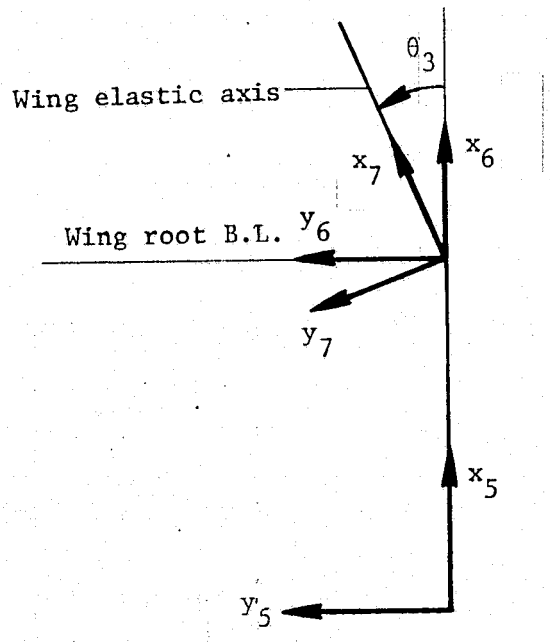

Sketch 5.- Fuselage-wing junction.

At the wing elastic axis/wing carry-through elastic axis junction:

$$\begin{Bmatrix} x \\ y \\ z \\ \alpha \\ \beta \\ \gamma \end{Bmatrix}_6 = \left[\begin{array}{c|c} [T_3] & [0] \\ \hline [0] & [T_3] \end{array}\right] \begin{Bmatrix} x \\ y \\ z \\ \alpha \\ \beta \\ \gamma \end{Bmatrix}_7 \tag{31}$$

where

$$\begin{Bmatrix} x \\ y \\ z \\ \alpha \\ \beta \\ \gamma \end{Bmatrix}_6 = \begin{Bmatrix} q_{47} \\ q_{48} \\ q_{49} \\ q_{50} \\ q_{51} \\ q_{52} \end{Bmatrix} \qquad \begin{Bmatrix} x \\ y \\ z \\ \alpha \\ \beta \\ \gamma \end{Bmatrix}_7 = \begin{Bmatrix} q_{88} \\ q_{67} \\ q_{53} \\ q_{81} \\ -q_{60} \\ q_{74} \end{Bmatrix} \tag{32}$$

and

$$[T_3] = \begin{bmatrix} \cos\theta_3 & -\sin\theta_3 & 0 \\ \sin\theta_3 & \cos\theta_3 & 0 \\ 0 & 0 & 1 \end{bmatrix} \tag{33}$$

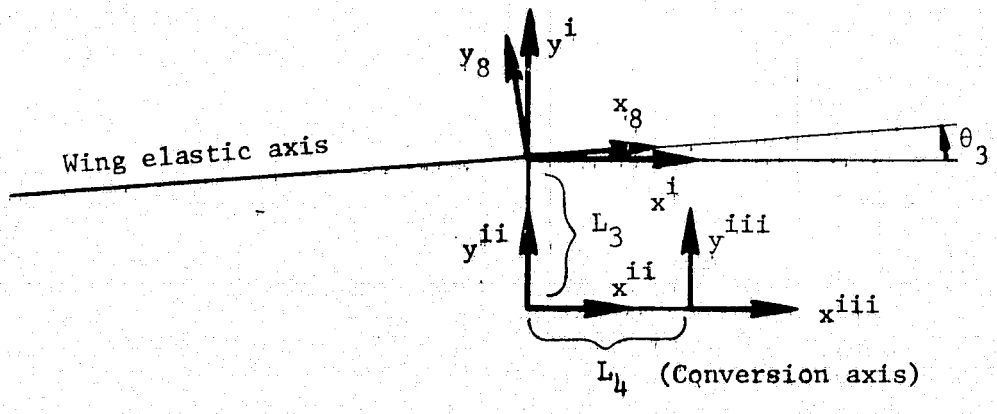

Sketch 6.- Geometry of wing/pylon junction.

The conversion axis is the centerline of the pylon conversion spindle which provides for tilting of the pylon. The geometric offset between the points of intersection of the wing elastic axis and the conversion axis with the wing tip rib (distance L_3 in the sketch #6) is taken to be rigid. The conversion axis, represented by the distance L_4 in sketch #6, is also assumed to be rigid. These rigidities are introduced by writing equations of constraint which relate coordinates $\{X\}^{iii}$ to coordinates $\{X\}_8$. The sequence of steps in establishing these equations follow.

An expression relating the coordinates at the last wing elastic axis station, $\{X\}_8$, to the intermediate (auxiliary) coordinates $\{X\}^i$ is given by

$$\begin{Bmatrix} x \\ y \\ z \\ \alpha \\ \beta \\ \gamma \end{Bmatrix}_8 = \left[\begin{array}{c|c} [T_4] & [0] \\ \hline [0] & [T_4] \end{array}\right] \begin{Bmatrix} x \\ y \\ z \\ \alpha \\ \beta \\ \gamma \end{Bmatrix}^i \equiv [R_4]\{X\}^i \tag{34}$$

where $\{X\}_8$ and $[T_4]$ are given by

$$\begin{Bmatrix} x \\ y \\ z \\ \alpha \\ \beta \\ \gamma \end{Bmatrix}_8 = \begin{Bmatrix} q_{88} \\ q_{73} \\ q_{59} \\ q_{87} \\ -q_{66} \\ q_{80} \end{Bmatrix} \tag{35}$$

and

$$\left[T_4\right] = \begin{bmatrix} \cos\theta_3 & \sin\theta_3 & 0 \\ -\sin\theta_3 & \cos\theta_3 & 0 \\ 0 & 0 & 1 \end{bmatrix} \tag{36}$$

As pointed out earlier, the auxiliary coordinates $\{X\}^i$ are not degrees of freedom but are introduced for convenience in arriving at the equations of constraint. From sketch #6 above, the intermediate coordinate vectors $\{X\}^i$ and $\{X\}^{ii}$ are seen to be related as

$$\begin{Bmatrix} x \\ y \\ z \\ \alpha \\ \beta \\ \gamma \end{Bmatrix}^i = \left[\begin{array}{ccc|ccc} 1 & 0 & 0 & 0 & 0 & -L_3 \\ 0 & 1 & 0 & 0 & 0 & 0 \\ 0 & 0 & 1 & L_3 & 0 & 0 \\ \hline 0 & 0 & 0 & 1 & 0 & 0 \\ 0 & 0 & 0 & 0 & 1 & 0 \\ 0 & 0 & 0 & 0 & 0 & 1 \end{array}\right] \begin{Bmatrix} x \\ y \\ z \\ \alpha \\ \beta \\ \gamma \end{Bmatrix}^{ii} \equiv [L_3]\{X\}^{ii} \tag{37}$$

If the conversion axis (length L_4 in the sketch #6) is taken to be flexible and treated as a beam-spring

$$\{X\}^{ii} = \{Q\}_{CA_I} \tag{38}$$

where $\{Q\}_{CA_I}$ is a column vector containing the degrees of freedom associated with the inboard end of the conversion axis beam-spring. The appropriate constraint equations would then have the matrix form

$$\{X\}_8 = [R_4]\,[L_3]\,\{Q\}_{CA_I} \tag{39}$$

Similarly, at the outboard end of the beam-spring representing the conversion axis

$$\{X\}^{iii} = \{Q\}_{CA_O} \tag{40}$$

where $\{Q\}_{CA_O}$ is a column vector containing the degrees of freedom for the outboard end. If the conversion axis is taken as rigid $\{X\}^{ii}$ and $\{X\}^{iii}$ would not be identified with degrees of freedom but would be auxiliary coordinates related according to

$$\begin{Bmatrix} x \\ y \\ z \\ \alpha \\ \beta \\ \gamma \end{Bmatrix}^{ii} = \left[\begin{array}{ccc|ccc} 1 & 0 & 0 & 0 & 0 & 0 \\ 0 & 1 & 0 & 0 & 0 & -L_4 \\ 0 & 0 & 1 & 0 & L_4 & 0 \\ \hline 0 & 0 & 0 & 1 & 0 & 0 \\ 0 & 0 & 0 & 0 & 1 & 0 \\ 0 & 0 & 0 & 0 & 0 & 1 \end{array}\right] \begin{Bmatrix} x \\ y \\ z \\ \alpha \\ \beta \\ \gamma \end{Bmatrix}^{iii} \equiv [L_4]\{X\}^{iii} \tag{41}$$

Herein, the conversion axis is assumed to be rigid so that equation 41 is applicable.

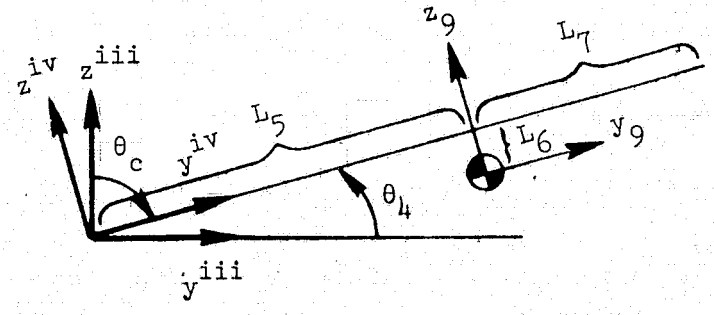

Sketch 7.- Junction of rotor shaft axis and conversion axis.

The pylon structure, consisting of the transmission/engine assembly, is treated as rigid. The intermediate coordinate vector $\{X\}^{iii}$ at the outboard end of the conversion axis is related to the coordinate vector $\{X\}^{iv}$ situated on the proprotor shaft axis according to

$$\{X\}^{iii} = \left[\begin{array}{c|c} [T_5] & [0] \\ \hline [0] & [T_5] \end{array}\right] \{X\}^{iv} \equiv [R_5]\{X\}^{iv} \tag{42}$$

where

$$[T_5] = \begin{bmatrix} 1 & 0 & 0 \\ 0 & \cos\theta_4 & -\sin\theta_4 \\ 0 & \sin\theta_4 & \cos\theta_4 \end{bmatrix} \tag{43}$$

The intermediate coordinate vector $\{X\}^{iv}$ is related to the pylon center-of-gravity coordinate vector $\{X\}_9$ by

$$\begin{Bmatrix} x \\ y \\ z \\ \alpha \\ \beta \\ \gamma \end{Bmatrix}^{iv} = \left[\begin{array}{ccc:ccc} 1 & 0 & 0 & 0 & L_6 & L_5 \\ 0 & 1 & 0 & -L_6 & 0 & 0 \\ 0 & 0 & 1 & -L_5 & 0 & 0 \\ \hdashline 0 & 0 & 0 & 1 & 0 & 0 \\ 0 & 0 & 0 & 0 & 1 & 0 \\ 0 & 0 & 0 & 0 & 0 & 1 \end{array}\right] \begin{Bmatrix} x \\ y \\ z \\ \alpha \\ \beta \\ \gamma \end{Bmatrix}_9 = [L_{5,6}]\{X\}_9 \tag{44}$$

where

$$\begin{Bmatrix} x \\ y \\ z \\ \alpha \\ \beta \\ \gamma \end{Bmatrix}_9 = \begin{Bmatrix} q_{89} \\ q_{90} \\ q_{91} \\ q_{92} \\ -q_{93} \\ q_{94} \end{Bmatrix} \tag{45}$$

On the basis of considerations in the preceding subsection and directly above, $\{X\}_8$ and $\{X\}_9$ are thus related according to

$$\{X\}_8 = [R_4]\,[L_3]\,[L_4]\,[R_5]\,[L_{5,6}]\,\{X\}_9 \tag{46}$$

The coordinate vectors $\{X\}_9$ and $\{X\}_{10}$ are related as

$$\begin{Bmatrix} x \\ y \\ z \\ \alpha \\ \beta \\ \gamma \end{Bmatrix}_9 = \left[\begin{array}{ccc|ccc} 0 & -1 & 0 & -L_6 & 0 & L_7 \\ 1 & 0 & 0 & 0 & -L_6 & 0 \\ 0 & 0 & 1 & 0 & L_7 & 0 \\ \hline 0 & 0 & 0 & 0 & -1 & 0 \\ 0 & 0 & 0 & 1 & 0 & 0 \\ 0 & 0 & 0 & 0 & 0 & 1 \end{array}\right] \begin{Bmatrix} x \\ y \\ z \\ \alpha \\ \beta \\ \gamma \end{Bmatrix}_{10} \tag{47}$$

where $\{X\}_{10}$, containing the degrees of freedom associated with the aft end of the beam-spring representing the mast, is given by

$$\begin{Bmatrix} x \\ y \\ z \\ \alpha \\ \beta \\ \gamma \end{Bmatrix}_{10} = \begin{Bmatrix} q_{95} \\ q_{96} \\ q_{97} \\ -q_{98} \\ -q_{99} \\ q_{100} \end{Bmatrix} \tag{48}$$

and $\{X\}_9$ has already been given in equation 45.

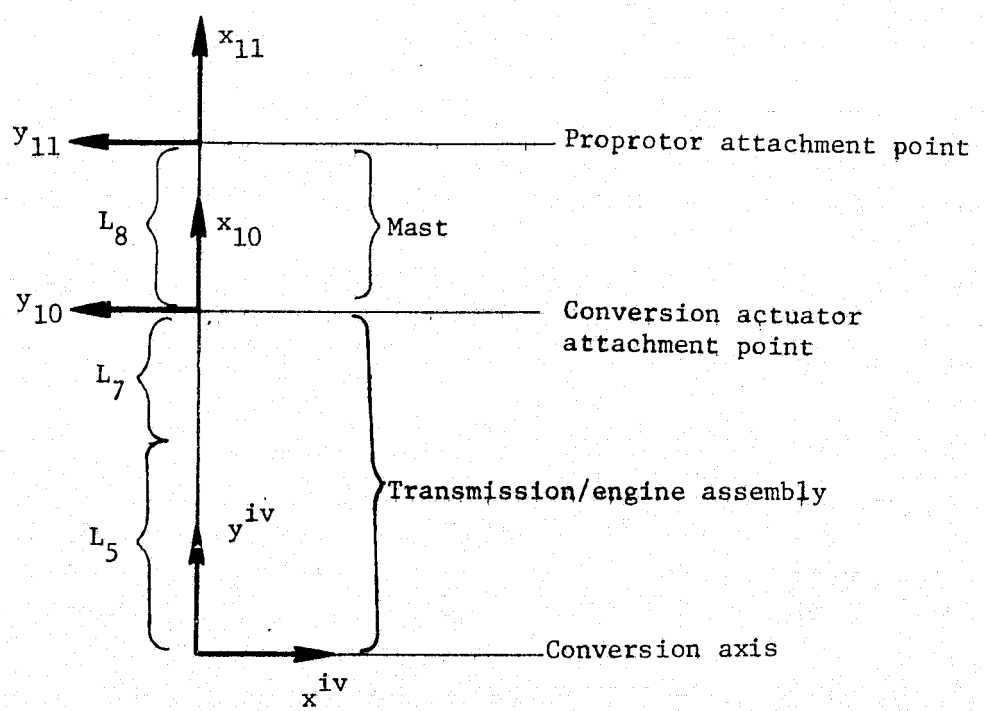

Sketch 8.- Geometry of pylon structure.

The pylon structure, consisting of the transmission and an underslung engine, is supported by the conversion axis and the conversion actuator which attaches

to the forward end of the transmission case. This is assumed to be rigid. The flexibility of the mast, the portion of the drive shaft extending forward of the transmission case on which the proprotor is mounted, is represented as a beam-spring. However, the only elastic deformations of the mast which will be considered are vertical and lateral bending, motion in the other two directions being solely of the rigid body type. At the forward end of the mast:

$$\begin{Bmatrix} x \\ y \\ z \\ \alpha \\ \beta \\ \gamma \end{Bmatrix}_{11} = \begin{Bmatrix} q_{101} \\ q_{102} \\ q_{103} \\ -q_{104} \\ -q_{105} \\ q_{106} \end{Bmatrix} \tag{49}$$

To suppress the longitudinal and torsional deformations of the mast while allowing rigid-body motions in these directions write

$$\begin{aligned} q_{101} - q_{95} &= 0 \\ q_{104} - q_{98} &= 0 \end{aligned} \tag{50}$$

These equations stipulate that the relative extensional and torsional deformations between the ends of the mast are zero.

The coordinates describing the proprotor disc, $\{X\}_R$, are taken in the same sense as $\{X\}_{11}$. Hence

$$\{X\}_R = \begin{Bmatrix} q_{107} \\ q_{108} \\ q_{109} \\ -q_{110} \\ -q_{111} \\ q_{112} \end{Bmatrix} \tag{51}$$

Assuming that the proprotor/hub combination is rigidly fastened to the mast, the constraint equations are given by

$$\{X\}_{11} = \{X\}_R \tag{52}$$

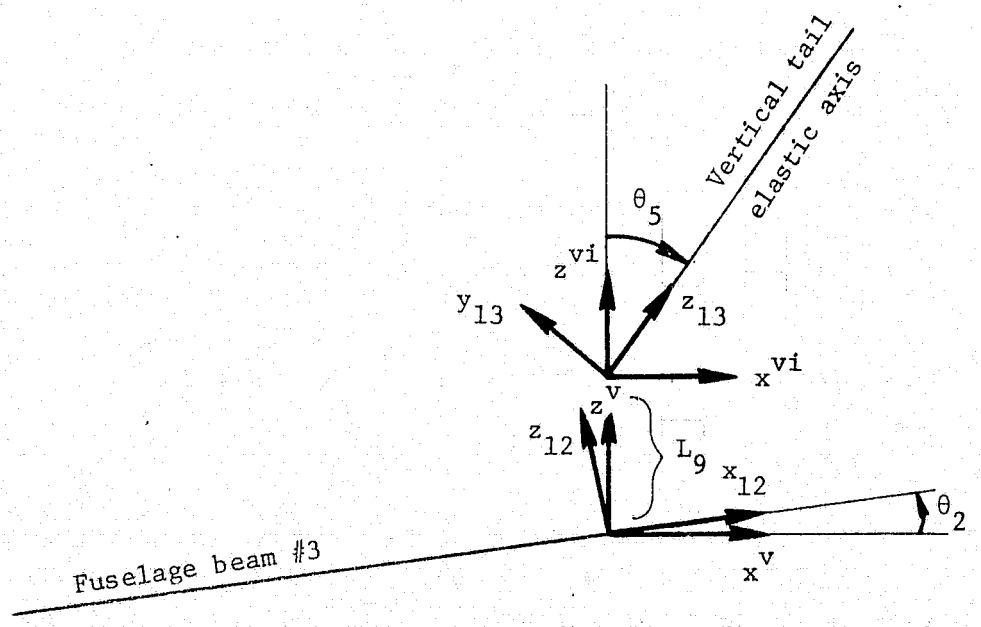

Sketch 9.- Attachment of vertical tail to fuselage beam #3.

At the aft end of fuselage beam #3

$$\begin{Bmatrix} x \\ y \\ z \\ \alpha \\ \beta \\ \gamma \end{Bmatrix}_{12} = \left[\begin{array}{c|c} [T_6] & [0] \\ \hline [0] & [T_6] \end{array}\right] \begin{Bmatrix} x \\ y \\ z \\ \alpha \\ \beta \\ \gamma \end{Bmatrix}^{v} \equiv [R_6]\{X\}^{v} \tag{53}$$

where

$$\begin{Bmatrix} x \\ y \\ z \\ \alpha \\ \beta \\ \gamma \end{Bmatrix}_{12} = \begin{Bmatrix} q_{41} \\ 0 \\ q_{32} \\ 0 \\ -q_{40} \\ 0 \end{Bmatrix} \tag{54}$$

and

$$[T_6] = \begin{bmatrix} \cos\theta_2 & 0 & \sin\theta_2 \\ 0 & 1 & 0 \\ -\sin\theta_2 & 0 & \cos\theta_2 \end{bmatrix} \tag{55}$$

Since the geometric offset between the fuselage and vertical tail elastic axes (distance L_9) is taken to be rigid the intermediate coordinate vectors $\{X\}^{v}$ and $\{X\}^{vi}$ are related according to

$$\begin{Bmatrix} x \\ y \\ z \\ \alpha \\ \beta \\ \gamma \end{Bmatrix}^{v} = \left[\begin{array}{ccc|ccc} 1 & 0 & 0 & 0 & -L_9 & \\ 0 & 1 & 0 & L_9 & 0 & 0 \\ 0 & 0 & 1 & & 0 & 0 \\ \hline 0 & 0 & 0 & 1 & 0 & 0 \\ 0 & 0 & 0 & 0 & 1 & 0 \\ 0 & 0 & 0 & 0 & 0 & 1 \end{array}\right] \begin{Bmatrix} x \\ y \\ z \\ \alpha \\ \beta \\ \gamma \end{Bmatrix}^{vi} \equiv [\, L_9 \,]\{X\}^{vi} \qquad (56)$$

At the base of the vertical tail elastic axis, $\{X\}^{vi}$ and $\{X\}_{13}$ are related as

$$\begin{Bmatrix} x \\ y \\ z \\ \alpha \\ \beta \\ \gamma \end{Bmatrix}^{vi} = \left[\begin{array}{c|c} [T_7] & [0] \\ \hline [0] & [T_7] \end{array}\right] \begin{Bmatrix} x \\ y \\ z \\ \alpha \\ \beta \\ \gamma \end{Bmatrix}_{13} \equiv [\, R_7 \,]\{X\}_{13} \qquad (57)$$

where

$$\begin{Bmatrix} x \\ y \\ z \\ \alpha \\ \beta \\ \gamma \end{Bmatrix}_{13} = \begin{Bmatrix} 0 \\ q_{13} \\ q_{123} \\ -q_{118} \\ 0 \\ 0 \end{Bmatrix} \qquad (58)$$

and

$$[T_7] = \begin{bmatrix} 0 & -\cos\theta_5 & \sin\theta_5 \\ 1 & 0 & 0 \\ 0 & \sin\theta_5 & \cos\theta_5 \end{bmatrix} \tag{59}$$

Assembling the series of transformation matrices indicated above the constraint equation is given by

$$\{X\}_{12} = [R_6]\,[L_9]\,[R_7]\,\{X\}_{13} \tag{60}$$

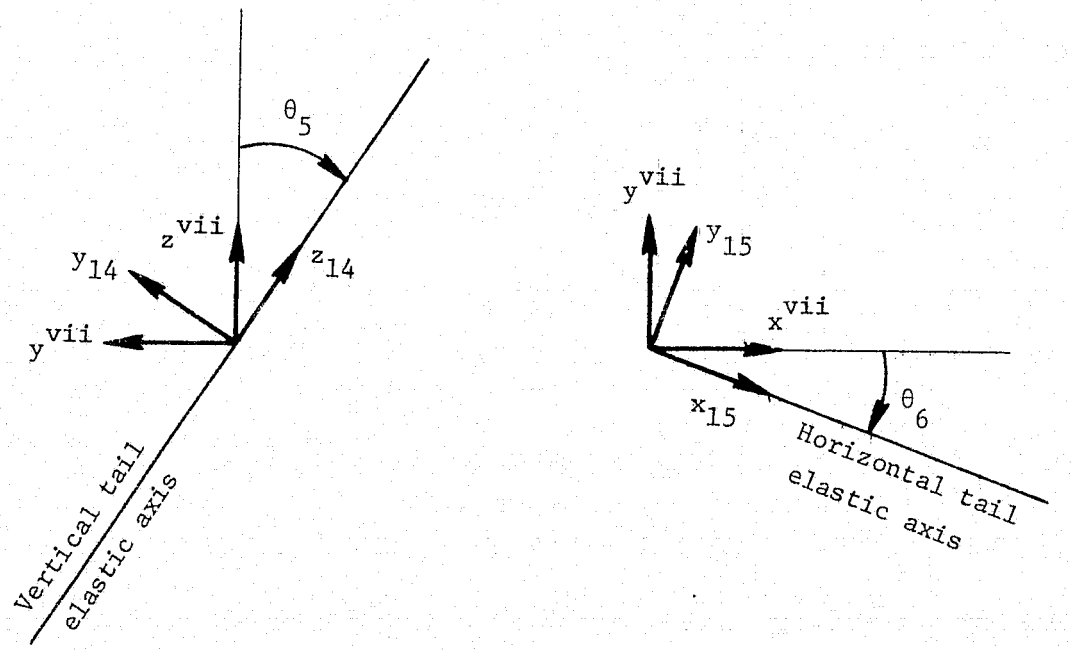

Sketch 10.- Attachment of horizontal tail to vertical tail.

At the junction of the vertical and horizontal tail elastic axes, $\{X\}_{14}$ and $\{X\}^{vii}$ are related as

$$\begin{Bmatrix} x \\ y \\ z \\ \alpha \\ \beta \\ \gamma \end{Bmatrix}_{14} = \left[\begin{array}{c|c} [T_8] & [0] \\ \hline [0] & [T_8] \end{array}\right] \begin{Bmatrix} x \\ y \\ z \\ \alpha \\ \beta \\ \gamma \end{Bmatrix}^{vii} \equiv [R_8]\{X\}^{vii} \tag{61}$$

where

$$\begin{Bmatrix} x \\ y \\ z \\ \alpha \\ \beta \\ \gamma \end{Bmatrix}_{14} = \begin{Bmatrix} 0 \\ q_{115} \\ q_{123} \\ -q_{120} \\ 0 \\ 0 \end{Bmatrix} \tag{62}$$

and

$$[T_8] = \begin{bmatrix} 1 & 0 & 0 \\ 0 & \cos\theta_5 & \sin\theta_5 \\ 0 & -\sin\theta_5 & \cos\theta_5 \end{bmatrix} \tag{63}$$

while $\{X\}^{vii}$ and $\{X\}_{15}$ are related according to

$$\begin{Bmatrix} x \\ y \\ z \\ \alpha \\ \beta \\ \gamma \end{Bmatrix}^{vii} = \left[\begin{array}{c|c} [T_9] & [0] \\ \hline [0] & [T_9] \end{array}\right] \begin{Bmatrix} x \\ y \\ z \\ \alpha \\ \beta \\ \gamma \end{Bmatrix}_{15} \equiv [R_9]\{X\}_{15} \tag{64}$$

with $\{X\}_{15}$ and $[T_9]$ being given by

$$\begin{Bmatrix} x \\ y \\ z \\ \alpha \\ \beta \\ \gamma \end{Bmatrix}_{15} = \begin{Bmatrix} q_{144} \\ q_{132} \\ q_{124} \\ q_{140} \\ -q_{128} \\ q_{136} \end{Bmatrix} \tag{65}$$

and

$$[T_9] = \begin{bmatrix} \cos\theta_6 & \sin\theta_6 & 0 \\ -\sin\theta_6 & \cos\theta_6 & 0 \\ 0 & 0 & 1 \end{bmatrix} \tag{66}$$

Equations 61 and 64 imply the matrix relation

$$\{X\}_{14} \equiv [R_8]\,[R_9]\,\{X\}_{15} \tag{67}$$

This completes the derivation of the equations of constraint for the symmetric formulation. For easy reference these equations are summarized in Table 8. Since there are 49 constraint equations and 144 degrees of freedom, the matrix of coefficients of the constraint equations ([C] of eqs. 4 and 5) will be of order 49 × 144.

It should be noted that one of the constraint equations involving q_{45} is redundant. (Compare eqs. 8 and 10 in Table 8.) In practice, such redundancies cannot be avoided and inadvertently appear in the equations of constraint, resulting in equations which are not linearly independent. Since such redundancies are not usually identifiable by inspection, special consideration must be accorded the constraint equations (ref. 22). The method advanced in reference 19 obviates the need to treat such redundant equations of constraint in any special manner. Since this method is employed in the computational procedure implemented in the SUDAN program which is used in the numerical example, the redundant equation will not (and need not) be deleted.

Structural properties of beam components.- The mass and stiffness matrices for the beams employed to represent the fuselage, wing, and empennage structures are established by substituting the data contained in Tables 1 to 3 into the appropriate matrix expressions developed earlier. The bending and torsion stiffness matrices follow from equations 6 and 11, respectively, while the lumped-mass inertia matrices, including wing and tail static unbalance, assume the form given in figure 9. Since the generation of these matrices using the data of Tables 1 to 3 is straightforward, the final numerical results are not shown.

Structural properties of rigid body components.-

Wing carry-through: Although the elasticity of the wing carry-through structure is included, its inertial properties are treated as though it were

rigid and combined with the inertia matrix of fuselage beam #2 by treating the center of gravity of the carry-through structure as rigidly attached to the last (right-hand) station of that beam. Assuming that the principal body axes at the center of gravity of the carry-through structure are parallel to axes x_3, y_3, and z_3, the kinetic energy of the carry-through structure in terms of the motion of its point of attachment is given by

$$T = \frac{1}{2}M\left(\dot{x}_3^2 + \dot{z}_3^2\right) + ML_1\dot{\beta}_3\dot{x}_3 + \frac{1}{2}\left[RI + ML_1^2\right]\dot{\beta}_3^2 \tag{68}$$

where use has been made of the development shown in figure 10. Substituting equation 68 into Lagrange's equation and then making use of the appropriate data in Tables 4 and 6 and equation 24 yields

$$[M]_{C-T} = \begin{array}{c} \begin{array}{ccc} q_{17} & q_{23} & q_{24} \end{array} \\ \begin{bmatrix} 154.1 & 0 & 0 \\ 0 & 2.93\text{x}10^6 & -1.81\text{x}10^4 \\ 0 & -1.81\text{x}10^4 & 154.1 \end{bmatrix} \end{array} \begin{array}{c} q_{17} \\ q_{23} \\ q_{24} \end{array} \tag{69}$$

as the matrix of additional terms to be added to the diagonal inertia matrix of fuselage beam #2.

Pylon: As indicated earlier, the rigid-body inertial properties of the pylon are defined relative to a coordinate axis system at the center-of-gravity. Hence, the pylon inertia matrix follows directly from Table 4 and has the form

$$[M]_{Pylon} = \begin{bmatrix} q_{89} & q_{90} & q_{91} & q_{92} & q_{93} & q_{94} \end{bmatrix} \begin{bmatrix} 1269.7 & & & & & \\ & 1269.7 & & & & \\ & & 1269.7 & & & \\ & & & 7.85\times10^{6} & & \\ & & & & 4.29\times10^{6} & \\ & & & & & 6.91\times10^{6} \end{bmatrix} \begin{bmatrix} q_{89} \\ q_{90} \\ q_{91} \\ q_{92} \\ q_{93} \\ q_{94} \end{bmatrix} \tag{70}$$

where the minus sign associated with q_{93} (cf. eq. 45) has been absorbed into the inertia matrix. The corresponding stiffness matrix is null.

Proprotor: The proprotor is treated as a rigid circular disc. Since the coordinate axes at the center of gravity of the proprotor disc are oriented such that they are principal axes the inertia matrix is diagonal and can be constructed directly from the data supplied in Table 4:

$$[M]_{Rotor} = \begin{bmatrix} q_{107} & q_{108} & q_{109} & q_{110} & q_{111} & q_{112} \end{bmatrix} \begin{bmatrix} 637.4 & & & & & \\ & 637.4 & & & & \\ & & 637.4 & & & \\ & & & 3.22\times10^{7} & & \\ & & & & 1.61\times10^{7} & \\ & & & & & 1.61\times10^{7} \end{bmatrix} \begin{bmatrix} q_{107} \\ q_{108} \\ q_{109} \\ q_{110} \\ q_{111} \\ q_{112} \end{bmatrix} \tag{71}$$

The matrix elements not shown are zero. The minus signs associated with q_{110} and q_{111} (cf. eq. 51) have been absorbed into the inertia matrix. The companion stiffness matrix is null since the proprotor hub is taken to be rigidly

attached to the mast. This matrix would not be null if the hub were spring-connected to the mast, as will be demonstrated below.

Structural properties of spring components.-

Wing carry-through: Since x_5 has been set to zero (cf. eq. 27) the beam-spring stiffness matrix is of order 11 × 11 and is given by that in figure 5 with the first row and column deleted. This matrix is shown in figure 20 along with the ordering of the degrees of freedom. Tables 5 and 6 contain the necessary data to evaluate the terms of the matrix. Constraint equations 29 and 30 in conjunction with the 11 × 11 stiffness matrix given in figure 20 imply that twisting and both the elastic and rigid-body axial motions of the beam-spring representing the wing carry-through structure are removed as degrees of freedom, in accordance with earlier discussions.

Pylon mast: The stiffness matrix of the pylon mast beam-spring is given in figure 21 along with the ordering of the degrees of freedom. Again, Tables 5 and 6 contain the data required to evaluate the individual terms of the matrix.

Some comments are included here to indicate the manner of treating a proprotor/hub assembly which is connected to the mast by springs. For illustrative purposes assume that the proprotor/hub combination is allowed to flap longitudinally and laterally with respect to the mast, the flapping motion being restrained by rotational springs K_{a_1} and K_{b_1}, respectively. Since longitudinal and lateral angular motions of the proprotor disc relative to the mast are permitted constraint equations 39 and 40 in Table 8 must be deleted. Recalling the treatment of springs in the spring-mass analogy employed earlier to illustrate the manner of including fuel slosh in a launch vehicle vibration analysis, an expression for the strain energy stored in the springs is required. The appropriate expression here is given by

$$V = \frac{1}{2} K_{a_1} \left(q_{105} - q_{111}\right)^2 + \frac{1}{2} K_{b_1} \left(q_{106} - q_{112}\right)^2 \tag{72}$$

Substituting equation 72 into Lagrange's equation then leads to

$$[\Delta K] = \begin{array}{c} \begin{array}{cccc} q_{105} & q_{106} & q_{111} & q_{112} \end{array} \\ \begin{bmatrix} K_{a_1} & 0 & -K_{a_1} & 0 \\ 0 & K_{b_1} & 0 & -K_{b_1} \\ -K_{a_1} & 0 & K_{a_1} & 0 \\ 0 & -K_{b_1} & 0 & K_{b_1} \end{bmatrix} \end{array} \begin{array}{c} \\ \begin{bmatrix} q_{105} \\ q_{106} \\ q_{111} \\ q_{112} \end{bmatrix} \end{array} \tag{73}$$

as the matrix of spring terms to be added to the partitioned system stiffness matrix, $[\overline{K}]$. For the coordinate numbering shown in figure 19, it is to be noted that the off-diagonal terms in equation 73 will couple the stiffness matrices for the pylon mast and proprotor substructures.

Anti-Symmetric Formulation

The considerations related to the symmetric formulation have illustrated the manner of establishing substructure mass and stiffness matrices and the mechanics of setting down equations of constraint. A corresponding derivation for the anti-symmetric case would, for the most part, be repetitious. For this reason a summary-type treatment, listing only final results which are different from the symmetric case, is given here.

For the anti-symmetric analysis the airframe motions considered are side bending and torsion of the fuselage and vertical tail and bending and torsion of the wing and horizontal tail. The same substructures and stations used in the symmetric analysis are employed here, leading to a problem having 165 degrees of freedom. The substructures are identified in figure 22 and the pertinent degrees of freedom in Table 9.

Constraint equations.- For anti-symmetric motions of the airframe the twist of the wing carry-through structure was judged to be important and the beam-spring representing it now also being permitted freedom in twist. Although extensional deformations of the wing carry-through are still negligible the ability to translate axially as rigid body must be provided for. The final constraint equations, 48 in number, are summarized in Table 10. The matrix of coefficients of the constraint equations ([C] of eqs. 4 and 5) is thus of order 48 × 165.

Structural properties of beam components.- As in the symmetric case the mass and stiffness matrices for the beams employed to represent the fuselage, wing, and empennage structures are established by substituting the data in Tables 1 to 3 into the appropriate matrix expressions developed earlier. Again, because the generation of these matrices is straightforward the final numerical results are not shown.

Structural properties of rigid body components.-

Wing carry-through: Here the vector $\{X\}_3$ is given by

$$\{X\}_3 = \begin{Bmatrix} 0 \\ q_{21} \\ 0 \\ q_{33} \\ 0 \\ q_{27} \end{Bmatrix} \tag{74}$$

so that

$$[M]_{C-T} = \begin{array}{c} \begin{array}{ccc} q_{21} & q_{27} & q_{33} \end{array} \\ \begin{bmatrix} 154.1 & 0 & -1.81\times10^{4} \\ 0 & 0 & 0 \\ -1.81\times10^{4} & 0 & 2.11\times10^{6} \end{bmatrix} \end{array} \begin{array}{c} \\ \begin{bmatrix} q_{21} \\ q_{27} \\ q_{33} \end{bmatrix} \end{array} \tag{75}$$

Pylon: The pylon inertia matrix is identical to that given by equation 70 for the symmetric case, with the degrees of freedom shown there, q_{89} through q_{94}, replaced by q_{106} through q_{111}, respectively.

Proprotor: The proprotor inertia matrix is identical to that given by equation 71 for the symmetric case, with the degrees of freedom shown there, q_{107} through q_{112}, replaced by q_{124} through q_{129}, respectively.

Structural properties of spring components.-

Wing carry-through: Since axial rigid-body motion of the carry-through is

included in the anti-symmetric formulation the beam-spring representing it has a stiffness matrix of order 12 × 12. Its form is the same as that given in figure 21. However, the degrees of freedom shown there, q_{95} through q_{106}, are replaced by q_{58} through q_{69}, respectively. Tables 5 and 6 contain the data needed to evaluate the individual terms of the matrix.

Pylon mast: The pylon mast beam-spring stiffness matrix is also given by figure 21 if q_{95} through q_{106} are replaced by q_{118} through q_{123}, respectively. Again Tables 5 and 6 provide the data required to evaluate the individual terms of the matrix.

Numerical Results

The direct method of analysis as embodied in the SUDAN program was used to calculate the symmetric and anti-symmetric free-free modes and frequencies for several pylon tilt angles. A summary of these frequencies for the first five elastic modes is given in Table 11. The first five symmetric modes for the case in which the pylons are tilted fully forward ($\theta_c = 90^o$) are sketched in figure 23. For reasons of both pictorial clarity and convenience, the changes in slope of the fuselage elastic axis and the offsets of the wing and vertical tail elastic axes from the fuselage elastic axis are not shown in the sketches. It should also be noted that while all degrees of freedom contribute to a coupled mode shape the shape is oftentimes dictated by the motion in a relatively few of the degrees of freedom. Such is the case here and only the predominant motion is indicated in the mode shape sketches given in figure 23.

CONCLUSIONS

The manner of representing a flight vehicle structure as an assembly of beam, spring, and rigid-body components for vibration analysis has been described. The development was couched in terms of a substructures methodology which is based on the finite-element stiffness method. Basic concepts were first introduced through several specific qualitative examples which included the modeling of wing structures, external stores, pylons supporting engines or external stores, and sprung masses associated with launch vehicle fuel slosh. A detailed numerical example consisting of a tilt-rotor VTOL aircraft was also given to provide an illustration of the procedures for modeling a structure, the manner of forming the substructure mass and stiffness matrices, and the mechanics of writing the equations of constraint which enforce deflection compatibility at the junctions of the substructures. Since many structures, or selected components, can be represented in this manner for vibration analysis, the modeling concepts described and their applications in the numerical example shown should prove generally useful to the dynamicist.

REFERENCES

1. Gieseke, R. K.: Modal Analysis of the Mated Space Shuttle Configuration. NASA TM X-2378, 1971, pp. 221-236.

2. Green, C. E.; Leadbetter, S. A.; and Rheinfurth, M. H.: Dynamic Testing for Shuttle Design Verification. NASA Space Shuttle Technology Conference, NASA TM X-2570, 1972, pp. 231-265.

3. Salus, W. L.; Jones, R. E.; and Ice, M. W.; Dynamic Analysis of a Long Span, Cable-Stayed Freeway Bridge Using NASTRAN, NASTRAN: User's Experiences, NASA TM X-2893, 1973, pp. 143-168.

4. Thornton, E. A.: Application of NASTRAN to a Space Shuttle Dynamics Model, NASTRAN: Users' Experiences, NASA TM X-2378, 1971, pp. 421-437.

5. McAleese, J. E.: Method for Determining Normal Modes and Frequencies of a Launch Vehicle Utilizing Its Component Normal Modes, NASA TN D-4550, May 1968.

6. Hayden, A. C. S.: Dynamic Response of Antenna Structures in a Launch Environment. Space Transportation System Technology Symposium. Vol. II — Dynamics and Aeroelasticity, NASA TM X-52876, 1970, pp. 301-329.

7. Jones, T. C.; and Pinson, L. D.: Adaptation of NASTRAN to the Analysis of the Viking Space Vehicle. NASTRAN: Users' Experiences, NASA TM X-2378, 1971, pp. 265-284.

8. Kenigsberg, I. J.: CH-53A Flexible Frame Vibration Analysis Test Correlation, Sikorsky Report SER 651195, 1973.

9. Ferman, M. A.: A Rapid Method for Flutter Clearance of Aircraft with External Stores. Technical Report AFFDL-TR-73-74, Vol. I, 1973.

10. Cronkhite, J. D.; Berry, V. L.; and Brunken, J. E.: A NASTRAN Vibration Model of the AH-1G Helicopter Airframe. Bell Helicopter Co., Report 209-099-432, 1974.

11. Anderson, W. D.; and Gaidelis, J. A.: Vibration Inputs and Response of a Hingeless Rotor Compound Helicopter, Lockheed Report LR 26523, June 1974.

12. Kvaternik, R. G.: Development and Applications of Two Computational Procedures for Determining the Vibration Modes of Structural Systems. NASA TN D-7995, November, 1975.

13. Martin, H. C.: Introduction to Matrix Methods of Structural Analysis. McGraw-Hill Book Co., New York, 1966.

14. Rubinstein, M. F.: Matrix Computer Analysis of Structures. Prentice-Hall, Inc., Englewood Cliffs, N.J., 1966.

15. Przemieniecki, J. S.: Theory of Matrix Structural Analysis. McGraw-Hill Book Co., New York, 1968.

16. Rubinstein, M. F.: Structural Systems — Statics, Dynamics and Stability, Prentice-Hall, Inc., Englewood Cliffs, New Jersey, 1970.

17. Martin, H. C.; and Carey, C. F.: Introduction to Finite Element Analysis. McGraw-Hill Book Co., New York, 1973.

18. Hurty, W. C.; and Rubinstein, M. F.: Dynamics of Structures. Prentice-Hall, Inc., Englewood Cliffs, N.J., 1964.

19. Walton, W. C., Jr.; and Steeves, E. C.: A New Matrix Theorem and Its Application for Establishing Independent Coordinates for Complex Dynamic Systems With Constraints. NASA TR R-326, October 1969.

20. Bauer, J. F.: Fluid Oscillations in the Containers of a Space Vehicle and Their Influence Upon Stability. NASA TR R-187, February 1964.

21. Anon.: Exploratory Definition Final Report, Model 266 Composite Aircraft Program, Vol. 7 — Dynamics, Report 266-099-207, Bell Helicopter Company, July 1967.

22. Greene, B. E.; Jones, R. E.; McLay, R. W.; and Strome, D. R.: Generalized Variational Principles in the Finite-Element Method. AIAA Journal, Vol. 7, July 1969, pp. 1254-1260.

TABLE 1.- FUSELAGE DISCRETIZATION

Station	Local Coordinate Position	Mass	Torsional Inertia	EI Vertical	EI Side	GJ
	(cm)	(kg)	(kg-cm^2)	(kN-cm^2)	(kN-cm^2)	(kN-cm^2)
Beam #1						
1	0.0	18.2	5.65×10^5	9.75×10^7	8.61×10^7	10.33×10^7
2	88.9	21.0	11.30	22.96	21.52	24.11
3	152.4	52.5	45.19	45.92	43.05	57.40
4	215.9	252.2	282.46	91.83	80.35	114.79
5	304.8	378.3	175.12	-----	-----	------
Beam #2						
1	0.0	378.3	175.12×10^5	229.58×10^7	129.14×10^7	200.89×10^7
2	101.6	924.7	420.30	390.29	218.10	246.80
3	190.5	357.2	271.16	459.17	269.76	252.54
4	254.0	42.0	124.28	476.39	286.98	252.54
5	304.8	168.1	259.86	482.13	298.46	254.54
6	355.6	147.1	175.12	------	------	------
Beam #3						
1	0.0	147.1	175.12×10^5	482.13×10^7	299.89×10^7	252.54×10^7
2	88.9	328.9	412.39	476.39	298.46	252.54
3	160.0	507.9	429.34	418.99	252.54	252.54
4	266.7	1849.3	463.24	258.28	172.19	232.45
5	381.0	447.6	463.24	129.14	114.79	172.19
6	477.5	126.1	101.68	86.09	80.35	114.79
7	596.9	61.3	67.79	51.66	51.08	74.61
8	729.0	105.1	45.19	------	------	------
Total Mass: Beam #1 = 722.2 kg, Beam #2 = 2017.4 kg, Beam #3 = 3573.3 kg						

TABLE 2.- WING DISCRETIZATION

Station	Local Coordinate Position	Mass	Static Unbalance*	Torsional Inertia About e.a.	EI Vertical	EI Chord	GJ
	(cm)	(kg)	(kg-cm)	(kg-cm^2)	(kN-cm^2)	(kN-cm^2)	(kN-cm^2)
1	0.0	154.3	-2304.	4.40×10^5	4.30×10^8	10.04×10^8	3.53×10^8
2	86.4	123.5	-2882.	4.68	3.56	8.60	2.98
3	190.5	90.7	-2188.	2.78	2.64	6.89	2.35
4	317.5	113.5	-2478.	2.61	1.72	5.16	1.72
5	439.4	62.5	-2882.	2.84	1.32	4.30	1.32
6	530.9	259.2	-4146.	5.94	1.19	4.08	1.20
7	563.9	0.0	0.	0.00	----	----	----

Total Mass = 803.6 kg

*Negative static unbalance indicates that section center of gravity is aft of section elastic axis.

TABLE 3.- EMPENNAGE DISCRETIZATION

Station	Local Coordinate Position	Mass	Static Unbalance*	Torsional Inertia About e.a.	EI Side	EI Chord	GJ
	(cm)	(kg)	(kg-cm)	(kg-cm^2)	(kN-cm^2)	(kN-cm^2)	(kN-cm^2)
Vertical Tail							
1	0.0	15.1	751.7	1.58×10^5	5.02×10^7	4.36×10^8	3.73×10^7
2	92.4	22.9	622.8	1.23	1.86	2.30	2.27
3	181.6	21.8	564.9	.98	.57	.98	1.15
4	274.3	20.4	467.1	.72	.29	.52	.52
5	368.3	14.6	353.6	.49	----	----	----
Total Mass = 94.9 kg							
Horizontal Tail							
1	0.0	0.0	0.0	0.0	1.29×10^7	$.86 \times 10^8$	1.15×10^7
2	88.9	0.0	0.0	0.0	.57	.43	.79
3	165.1	63.0	0.0	$.25 \times 10^5$	.34	.21	.29
4	254.0	0.0	0.0	0.0	----	----	----
Total Mass = 63.0 kg							

*Positive static unbalance indicates that section center of gravity is forward of section elastic axis.

TABLE 4.- INERTIAL PROPERTIES OF COMPONENTS TREATED AS RIGID

PROPROTOR	
Mass	637.4 kg
Flapping Inertia	
Longitudinal	1.6087×10^7 kg-cm^2
Lateral	1.6087×10^7 kg-cm^2
Polar Inertia	3.2174×10^7 kg-cm^2
PYLON	
Mass	1269.7 kg
C. G. Inertia	
Pitch	7.8524×10^6 kg-cm^2
Roll	4.2934×10^6 kg-cm^2
Yaw	6.9146×10^6 kg-cm^2
WING CARRY-THROUGH *	
Mass	154.1 kg
C. G. Inertia	
Pitch	8.1936×10^5 kg-cm^2
Roll	Not available
Yaw	Not available

*Treated as rigid inertially but not elastically

TABLE 5.- STIFFNESS PROPERTIES OF COMPONENTS TREATED AS SPRINGS

Wing Carry-Through*

$EI_{vertical}$	$= 4.5056 \times 10^8$ kN-cm^2
$EI_{lateral}$	$= 10.5898 \times 10^8$ kN-cm^2
GJ	$= 3.6733 \times 10^8$ kN-cm^2

Pylon Mast†

$EI_{vertical}$	$= 7.1745 \times 10^7$ kN-cm^2
$EI_{lateral}$	$= 7.1745 \times 10^7$ kN-cm^2

*AE is taken to be infinite

†Both AE and GJ are taken to be infinite

TABLE 6.- GEOMETRIC QUANTITIES EMPLOYED IN VIBRATION ANALYSIS

ANGLES

θ_1	9.5° (.1658 Radians)
θ_2	5.6° (.09774 Radians)
θ_3	4.5° (.07854 Radians)
θ_4	Varied
θ_5	25° (.4363 Radians)
θ_6	15° (.2618 Radians)

LENGTHS

L_1	117.1 cm
L_2	106.7 cm
L_3	43.2 cm
L_4	43.2 cm
L_5	79.2 cm
L_6	48.3 cm
L_7	60.4 cm
L_8	71.1 cm
L_9	38.1 cm

TABLE 7.- IDENTIFICATION OF DEGREES OF FREEDOM FOR SYMMETRIC VIBRATION ANALYSIS

FUSELAGE		
Beam #1		
$q_1 - q_5$	Displs.	Vertical Bending
$q_6 - q_{10}$	Slopes	
q_{11}	Axial rigid body	
Beam #2		
$q_{12} - q_{17}$	Displs.	Vertical Bending
$q_{18} - q_{23}$	Slopes	
q_{24}	Axial rigid body	
Beam #3		
$q_{25} - q_{32}$	Displs.	Vertical Bending
$q_{33} - q_{40}$	Slopes	
q_{41}	Axial rigid body	
Wing Carry-Through Structure		
$q_{42} - q_{52}$		
WING		
$q_{53} - q_{59}$	Displs.	Vertical Bending
$q_{60} - q_{66}$	Slopes	
$q_{67} - q_{73}$	Displs.	Fore and Aft Bending
$q_{74} - q_{80}$	Slopes	
$q_{81} - q_{87}$	Torsion	
q_{88}	Axial rigid body	

TABLE 7.- Concluded.

PYLON		
Transmission/Engine Assembly		
$q_{89} - q_{94}$	Rigid Body Translations and Rotations	
Mast		
$q_{95} - q_{106}$		
PROPROTOR		
$q_{107} - q_{112}$	Rigid Body Translations and Rotations	
EMPENNAGE		
Vertical Tail		
$q_{113} - q_{117}$	Displs	Fore and Aft Bending
$q_{118} - q_{122}$	Slopes	
q_{123}	Axial rigid body	
Horizontal Tail		
$q_{124} - q_{127}$	Displs.	Vertical Bending
$q_{128} - q_{131}$	Slopes	
$q_{132} - q_{135}$	Displs.	Fore and Aft Bending
$q_{136} - q_{139}$	Slopes	
$q_{140} - q_{143}$	Torsion	
q_{144}	Axial rigid body	

TABLE 8.- CONSTRAINT EQUATIONS FOR SYMMETRIC VIBRATION ANALYSIS

1. $q_{11} \cos \theta_1 - q_5 \sin \theta_1 - q_{24} = 0$
2. $q_{11} \sin \theta_1 + q_5 \cos \theta_1 - q_{12} = 0$
3. $-q_{10} + q_{18} = 0$
4. $q_{41} \cos \theta_2 - q_{25} \sin \theta_2 - q_{24} = 0$
5. $q_{41} \sin \theta_2 + q_{25} \cos \theta_2 - q_{17} = 0$
6. $-q_{33} + q_{23} = 0$
7. $q_{42} + L_1 q_{44} + q_{24} = 0$
8. $-L_1 q_{45} = 0$
9. $q_{43} - q_{17} = 0$
10. $-q_{45} = 0$
11. $q_{44} + q_{23} = 0$
12. $q_{46} = 0$
13. $q_{50} - q_{44} = 0$
14. $q_{47} = 0$
15. $q_{88} \cos \theta_3 - q_{67} \sin \theta_3 - q_{47} = 0$
16. $q_{88} \sin \theta_3 + q_{67} \cos \theta_3 - q_{48} = 0$
17. $q_{53} - q_{44} = 0$
18. $q_{81} \cos \theta_3 + q_{60} \sin \theta_3 - q_{50} = 0$
19. $q_{81} \sin \theta_3 - q_{60} \cos \theta_3 - q_{51} = 0$
20. $q_{74} - q_{52} = 0$
21. $q_{89} \cos \theta_3 + q_{90} \sin \theta_3 \cos \theta_4 - q_{91} \sin \theta_3 \sin \theta_4 + q_{92}\left[L_5 \sin \theta_3 \sin \theta_4 - L_6 \sin \theta_3 \cos \theta_4\right] - q_{93}\left[L_6 \cos \theta_3 - \sin \theta_4\left(L_4 \sin \theta_3 + L_3 \cos \theta_3\right)\right] + q_{94}\left[L_5 \cos \theta_3 - \cos \theta_4\left(L_4 \sin \theta_3 + L_3 \cos \theta_3\right)\right] - q_{88} = 0$

TABLE 8.- Continued

22. $-q_{89} \sin \theta_3 + q_{90} \cos \theta_3 \cos \theta_4 - q_{91} \cos \theta_3 \sin \theta_4 + q_{92}\left[L_5 \sin \theta_4 \cos \theta_3 - L_6 \cos \theta_3 \cos \theta_4\right] - q_{93}\left[-L_6 \sin \theta_3 + \sin \theta_4 \left(L_3 \sin \theta_3 - L_4 \cos \theta_3\right)\right] + q_{94}\left[-L_5 \sin \theta_3 + \cos \theta_4 \left(L_3 \sin \theta_3 - L_4 \cos \theta_3\right)\right] - q_{73} = 0$

23. $q_{92} \cos \theta_3 - q_{93} \sin \theta_3 \cos \theta_4 - q_{94} \sin \theta_3 \sin \theta_4 - q_{87} = 0$

24. $q_{90} \sin \theta_4 + q_{91} \cos \theta_4 + q_{92}\left[L_3 - L_5 \cos \theta_4 - L_6 \sin \theta_4\right] - q_{93} L_4 \cos \theta_4 - q_{94} L_4 \sin \theta_4 - q_{59} = 0$

25. $q_{92} \sin \theta_3 + q_{93} \cos \theta_3 \cos \theta_4 + q_{94} \cos \theta_3 \sin \theta_4 - q_{66} = 0$

26. $-q_{93} \sin \theta_4 + q_{94} \cos \theta_4 - q_{80} = 0$

27. $-q_{96} + L_7 q_{100} - q_{89} + L_6 q_{98} = 0$

28. $q_{95} - q_{90} + L_6 q_{99} = 0$

29. $q_{97} - L_7 q_{99} - q_{91} = 0$

30. $q_{99} - q_{92} = 0$

31. $-q_{98} + q_{93} = 0$

32. $q_{100} - q_{94} = 0$

33. $q_{101} - q_{95} = 0$

34. $q_{104} - q_{98} = 0$

35. $q_{107} - q_{101} = 0$

36. $q_{108} - q_{102} = 0$

37. $q_{109} - q_{103} = 0$

38. $-q_{110} + q_{104} = 0$

39. $-q_{111} + q_{105} = 0$

40. $q_{112} - q_{106} = 0$

41. $q_{113}\left[-\cos \theta_2 \cos \theta_5 + \sin \theta_2 \sin \theta_5\right] + q_{123}\left[\cos \theta_2 \sin \theta_5 + \sin \theta_2 \cos \theta_5\right] + q_{118} L_9 \cos \theta_2 - q_{41} = 0$

TABLE 8.- Concluded

42. $q_{113}\left[\sin\theta_2 \cos\theta_5 + \sin\theta_5 \cos\theta_2\right] + q_{123}\left[-\sin\theta_2 \sin\theta_5 + \cos\theta_2 \cos\theta_5\right] - q_{118} L_9 \sin\theta_2 - q_{32} = 0$

43. $-q_{118} + q_{40} = 0$

44. $q_{144} \cos\theta_6 + q_{132} \sin\theta_6 = 0$

45. $-q_{144} \cos\theta_5 \sin\theta_6 + q_{132} \cos\theta_5 \cos\theta_6 + q_{124} \sin\theta_5 - q_{115} = 0$

46. $q_{144} \sin\theta_5 \sin\theta_6 - q_{132} \sin\theta_5 \cos\theta_6 + q_{124} \cos\theta_5 - q_{123} = 0$

47. $q_{140} \cos\theta_6 - q_{128} \sin\theta_6 + q_{120} = 0$

48. $-q_{140} \cos\theta_5 \sin\theta_6 - q_{128} \cos\theta_5 \cos\theta_6 + q_{136} \sin\theta_5 = 0$

49. $q_{140} \sin\theta_5 \sin\theta_6 + q_{128} \sin\theta_5 \cos\theta_6 + q_{136} \cos\theta_5 = 0$

TABLE 9.- IDENTIFICATION OF DEGREES OF FREEDOM FOR ANTI-SYMMETRIC VIBRATION ANALYSIS

FUSELAGE		
Beam #1		
$q_1 - q_5$	Displs.	Side Bending
$q_6 - q_{10}$	Slopes	
$q_{11} - q_{15}$	Torsion	
Beam #2		
$q_{16} - q_{21}$	Displs.	Side Bending
$q_{22} - q_{27}$	Slopes	
$q_{28} - q_{33}$	Torsion	
Beam #3		
$q_{34} - q_{41}$	Displs.	Side Bending
$q_{42} - q_{49}$	Slopes	
$q_{50} - q_{57}$	Torsion	
Wing Carry-Through Structure		
$q_{58} - q_{69}$		
WING		
$q_{70} - q_{76}$	Displs.	Vertical Bending
$q_{77} - q_{83}$	Slopes	
$q_{84} - q_{90}$	Displs.	Fore and Aft Bending
$q_{91} - q_{97}$	Slopes	
$q_{98} - q_{104}$	Torsion	
q_{105}	Axial rigid body	

TABLE 9.- Concluded

PYLON		
Transmission/Engine Assembly		
$q_{106} - q_{111}$	Rigid Body Translations and Rotations	
Mast		
$q_{112} - q_{123}$		
PROPROTOR		
$q_{124} - q_{129}$	Rigid Body Translations and Rotations	
EMPENNAGE		
Vertical Tail		
$q_{130} - q_{134}$	Displs.	Side Bending
$q_{135} - q_{139}$	Slopes	
$q_{140} - q_{144}$	Torsion	
Horizontal Tail		
$q_{145} - q_{148}$	Displs.	Vertical Bending
$q_{149} - q_{152}$	Slopes	
$q_{153} - q_{156}$	Displs.	Fore and Aft Bending
$q_{157} - q_{160}$	Slopes	
$q_{161} - q_{164}$	Torsion	
q_{165}	Axial rigid body	

TABLE 10.- CONSTRAINT EQUATIONS FOR ANTI-SYMMETRIC VIBRATION ANALYSIS

1. $q_5 - q_{16} = 0$
2. $q_{15} \cos \theta_1 - q_{10} \sin \theta_1 - q_{28} = 0$
3. $q_{15} \sin \theta_1 + q_{10} \cos \theta_1 - q_{22} = 0$
4. $q_{34} - q_{21} = 0$
5. $q_{50} \cos \theta_2 - q_{42} \sin \theta_2 - q_{33} = 0$
6. $q_{50} \sin \theta_2 + q_{42} \cos \theta_2 - q_{27} = 0$
7. $q_{59} + L_1 q_{61} = 0$
8. $q_{58} - L_1 q_{62} - q_{21} = 0$
9. $q_{60} = 0$
10. $q_{62} + q_{33} = 0$
11. $q_{61} = 0$
12. $q_{63} - q_{27} = 0$
13. $q_{64} - q_{58} = 0$
14. $q_{105} \cos \theta_3 - q_{84} \sin \theta_3 - q_{64} = 0$
15. $q_{105} \sin \theta_3 + q_{84} \cos \theta_3 - q_{65} = 0$
16. $q_{70} - q_{66} = 0$
17. $q_{98} \cos \theta_3 + q_{77} \sin \theta_3 - q_{67} = 0$
18. $q_{98} \sin \theta_3 - q_{77} \cos \theta_3 - q_{68} = 0$
19. $q_{91} - q_{69} = 0$
20. $q_{106} \cos \theta_3 + q_{107} \sin \theta_3 \cos \theta_4 - q_{108} \sin \theta_3 \sin \theta_4 + q_{109}\left[L_5 \sin \theta_3 \sin \theta_4 - L_6 \sin \theta_3 \cos \theta_4\right] - q_{110}\left[L_6 \cos \theta_3 - \sin \theta_4\left(L_4 \sin \theta_3 + L_3 \cos \theta_3\right)\right] + q_{111}\left[L_5 \cos \theta_3 - \cos \theta_4\left(L_4 \sin \theta_3 + L_3 \cos \theta_3\right)\right] - q_{105} = 0$

TABLE 10.- Continued

21. $-q_{106} \sin \theta_3 + q_{107} \cos \theta_3 \cos \theta_4 - q_{108} \cos \theta_3 \sin \theta_4 + q_{109}\left[L_5 \sin \theta_4 \cos \theta_3 - L_6 \cos \theta_3 \cos \theta_4\right] - q_{110}\left[-L_6 \sin \theta_3 + \sin \theta_4\left(L_3 \sin \theta_3 - L_4 \cos \theta_3\right)\right] + q_{111}\left[-L_5 \sin \theta_3 + \cos \theta_4\left(L_3 \sin \theta_3 - L_4 \cos \theta_3\right)\right] - q_{90} = 0$

22. $q_{109} \cos \theta_3 - q_{110} \sin \theta_3 \cos \theta_4 - q_{111} \sin \theta_3 \sin \theta_4 - q_{104} = 0$

23. $q_{107} \sin \theta_4 + q_{108} \cos \theta_4 + q_{109}\left[L_3 - L_5 \cos \theta_4 - L_6 \sin \theta_4\right] - q_{110} L_4 \cos \theta_4 - q_{111} L_4 \sin \theta_4 - q_{76} = 0$

24. $-q_{109} \sin \theta_3 - q_{110} \cos \theta_3 \cos \theta_4 - q_{111} \cos \theta_3 \sin \theta_4 + q_{83} = 0$

25. $-q_{110} \sin \theta_4 + q_{111} \cos \theta_4 - q_{97} = 0$

26. $-q_{113} + L_7 q_{117} - q_{106} + L_6 q_{115} = 0$

27. $q_{112} - q_{107} + L_6 q_{116} = 0$

28. $q_{114} - L_7 q_{116} - q_{108} = 0$

29. $q_{116} - q_{109} = 0$

30. $-q_{115} + q_{110} = 0$

31. $q_{117} - q_{111} = 0$

32. $q_{118} - q_{112} = 0$

33. $q_{121} - q_{115} = 0$

34. $q_{124} - q_{118} = 0$

35. $q_{125} - q_{114} = 0$

36. $q_{126} - q_{120} = 0$

37. $-q_{127} + q_{121} = 0$

38. $-q_{128} + q_{122} = 0$

39. $q_{129} - q_{123} = 0$

40. $q_{130} - q_{135} L_9 \cos \theta_5 + q_{140} L_9 \sin \theta_5 - q_{41} = 0$

TABLE 10.- Concluded

41. $q_{135}\left[-\cos\theta_2\cos\theta_5 + \sin\theta_2\sin\theta_5\right] + q_{140}\left[\cos\theta_2\sin\theta_5 + \sin\theta_2\cos\theta_5\right] - q_{57} = 0$

42. $q_{135}\left[\sin\theta_2\cos\theta_5 + \cos\theta_2\sin\theta_5\right] + q_{140}\left[-\sin\theta_2\sin\theta_5 + \cos\theta_2\cos\theta_5\right] - q_{49} = 0$

43. $q_{165}\cos\theta_6 + q_{153}\sin\theta_6 - q_{132} = 0$

44. $-q_{165}\cos\theta_5\sin\theta_6 + q_{153}\cos\theta_5\cos\theta_6 + q_{145}\sin\theta_5 = 0$

45. $q_{165}\sin\theta_5\sin\theta_6 - q_{153}\sin\theta_5\cos\theta_6 + q_{145}\cos\theta_5 = 0$

46. $q_{161}\cos\theta_6 - q_{149}\sin\theta_6 = 0$

47. $-q_{161}\cos\theta_5\sin\theta_6 - q_{149}\cos\theta_5\cos\theta_6 + q_{157}\sin\theta_5 - q_{137} = 0$

48. $q_{161}\sin\theta_5\sin\theta_6 + q_{149}\sin\theta_5\cos\theta_6 + q_{157}\cos\theta_5 - q_{142} = 0$

TABLE 11.- FREE-FREE ELASTIC MODE FREQUENCIES OF MODEL 266 TILT-ROTOR (Hz)

Symmetric Mode Frequencies

Mode \ θ_c	0°	15°	30°	45°	60°	75°	90°
1	2.114	2.138	2.168	2.199	2.224	2.235	2.229
2	3.473	3.488	3.487	3.470	3.304	3.399	3.360
3	5.727	5.698	5.661	5.628	5.610	5.617	5.644
4	7.235	7.378	7.646	8.021	8.694	8.895	9.016
5	11.490	11.509	11.522	11.523	10.802	11.046	10.661

Anti-symmetric Mode Frequencies

Mode \ θ_c	0°	15°	30°	45°	60°	75°	90°
1	3.882	3.882	3.884	3.883	3.875	3.856	3.825
2	4.602	4.699	4.801	4.891	4.936	4.906	4.818
3	5.702	5.645	5.569	5.492	5.446	5.464	5.528
4	7.256	7.347	7.373	7.339	7.294	7.251	7.214
5	7.633	7.624	7.775	8.073	8.456	8.860	9.136

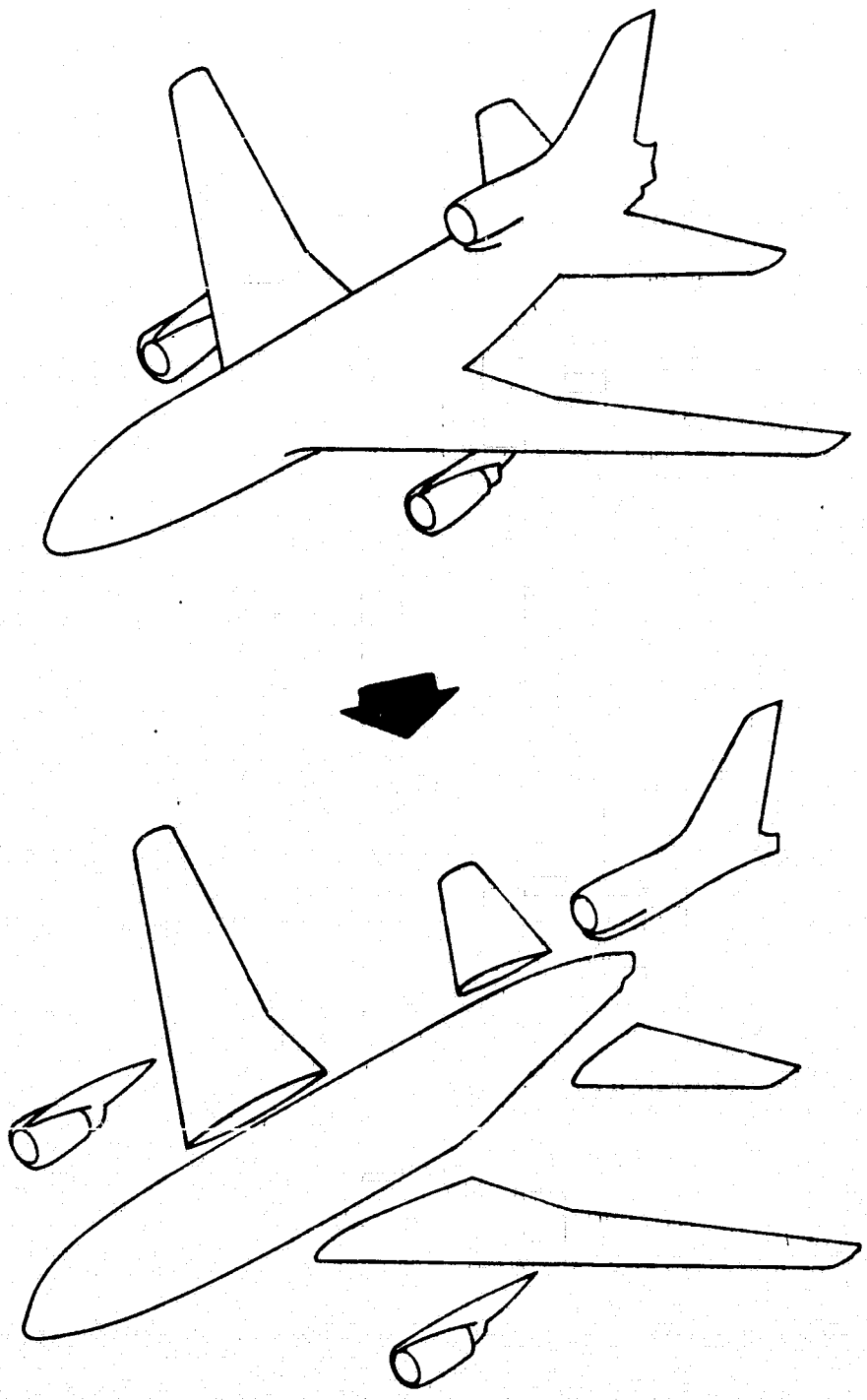

Figure 1.- Partitioning an aircraft structure into substructures.

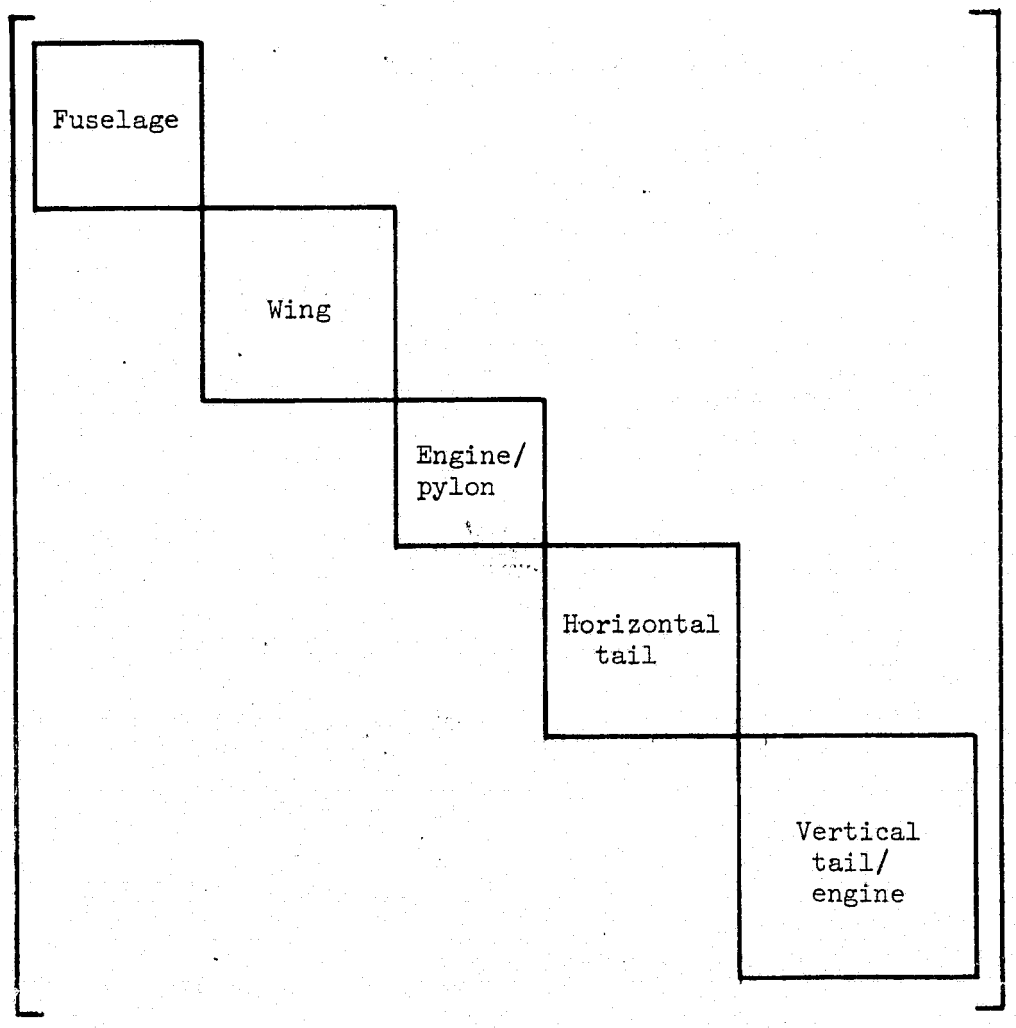

Figure 2.- Block diagonal composition of $[\overline{M}]$ and $[\overline{K}]$ for aircraft of figure 1.

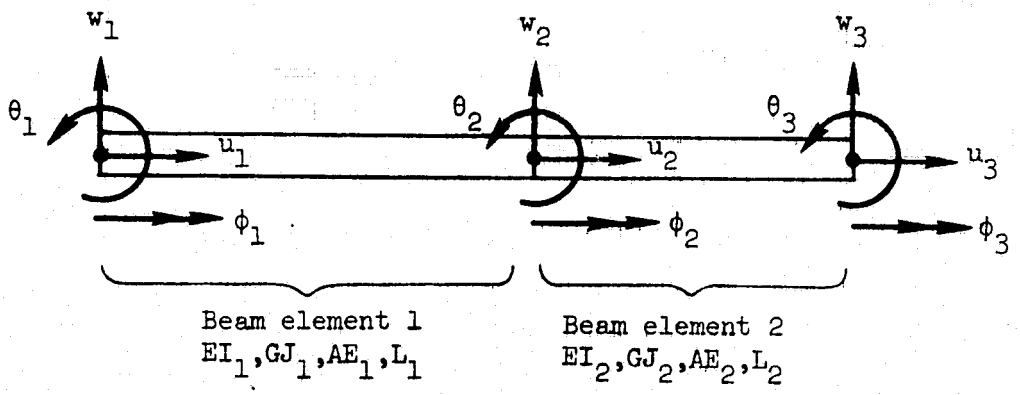

Figure 3.- A two-element beam substructure.

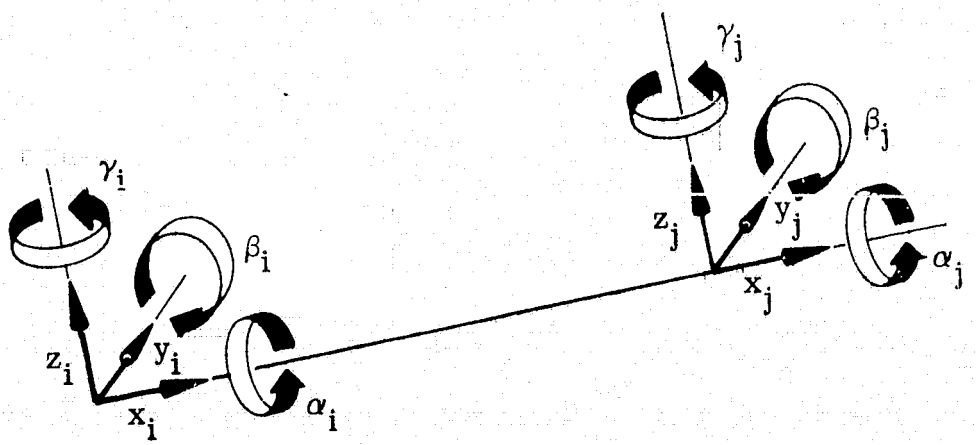

Figure 4.- Sign convention for end deflections of massless uniform beam segment (beam-spring).

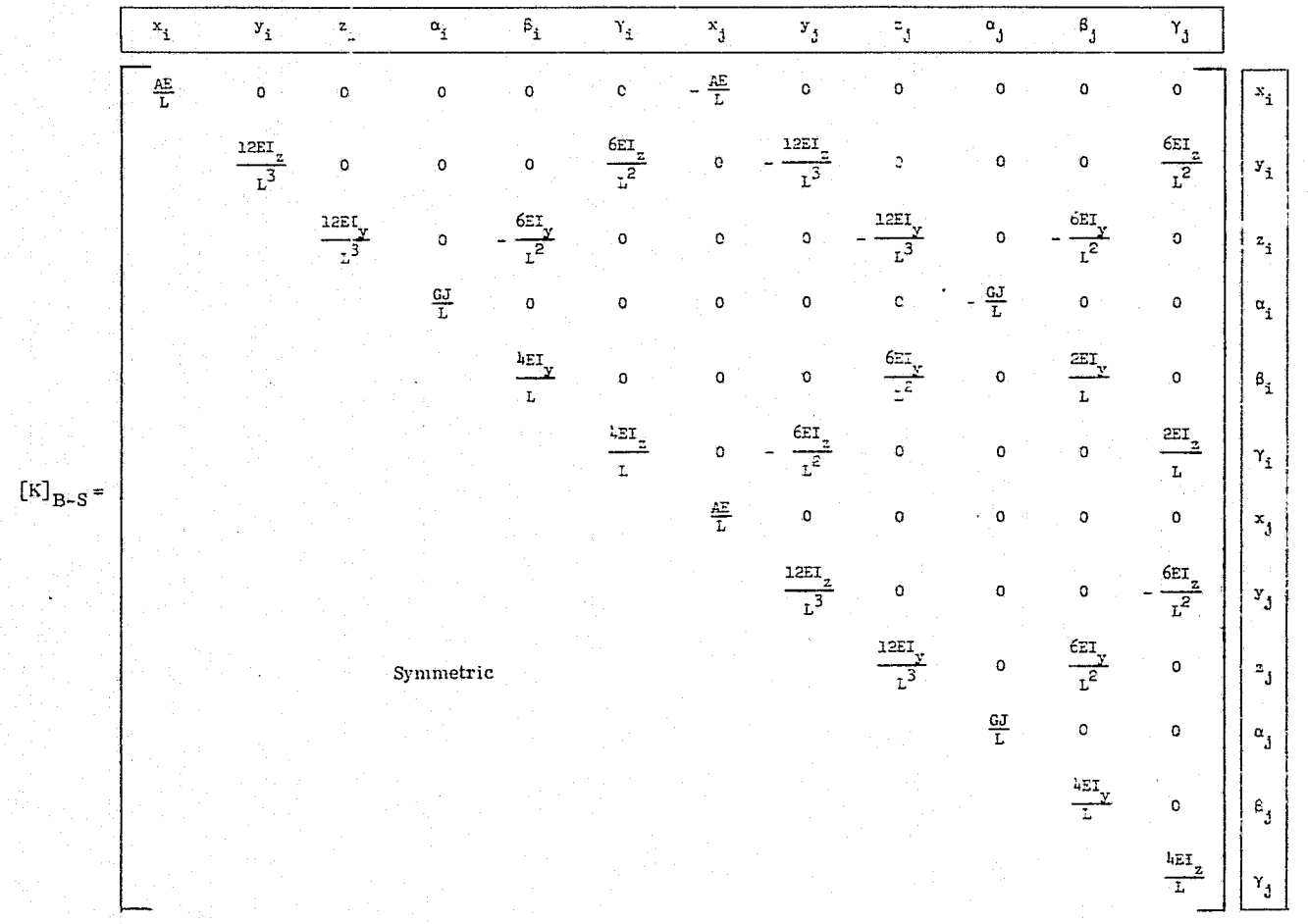

Figure 5.- Stiffness matrix of massless uniform beam segment (beam-spring).

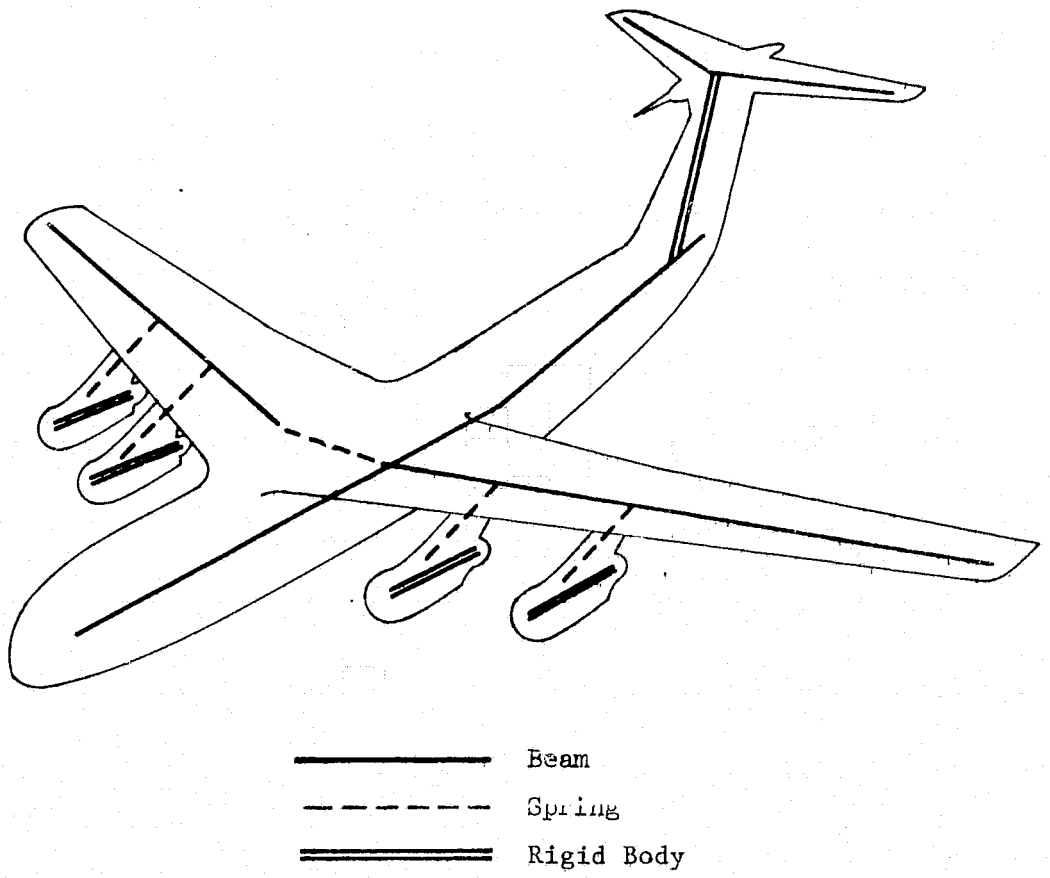

Figure 6.- "Stick" model of transport aircraft for symmetric vibration analysis.

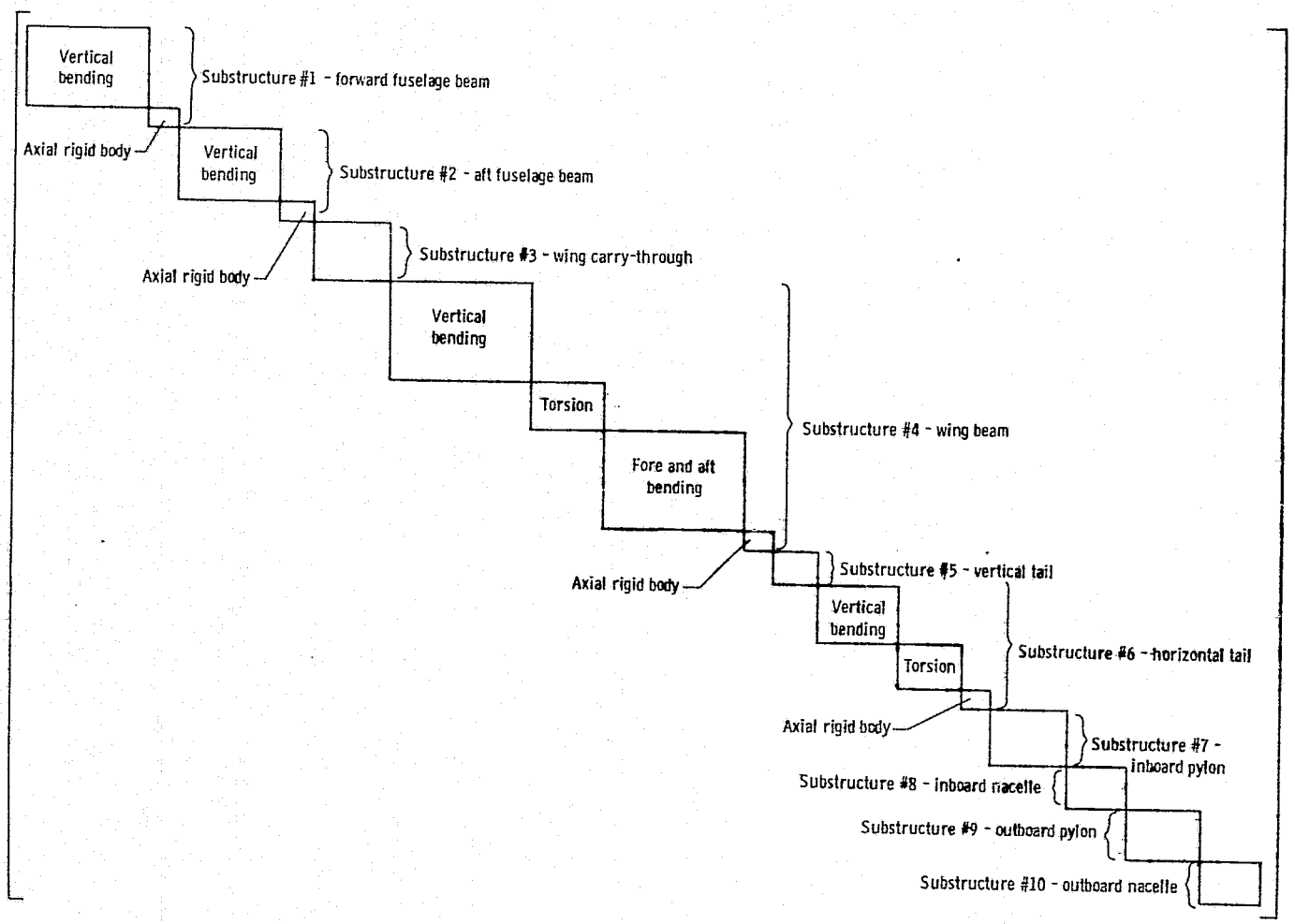

Figure 7.- Block diagonal composition of matrices $[\bar{M}]$ and $[\bar{K}]$ for the beam model of Figure 6.

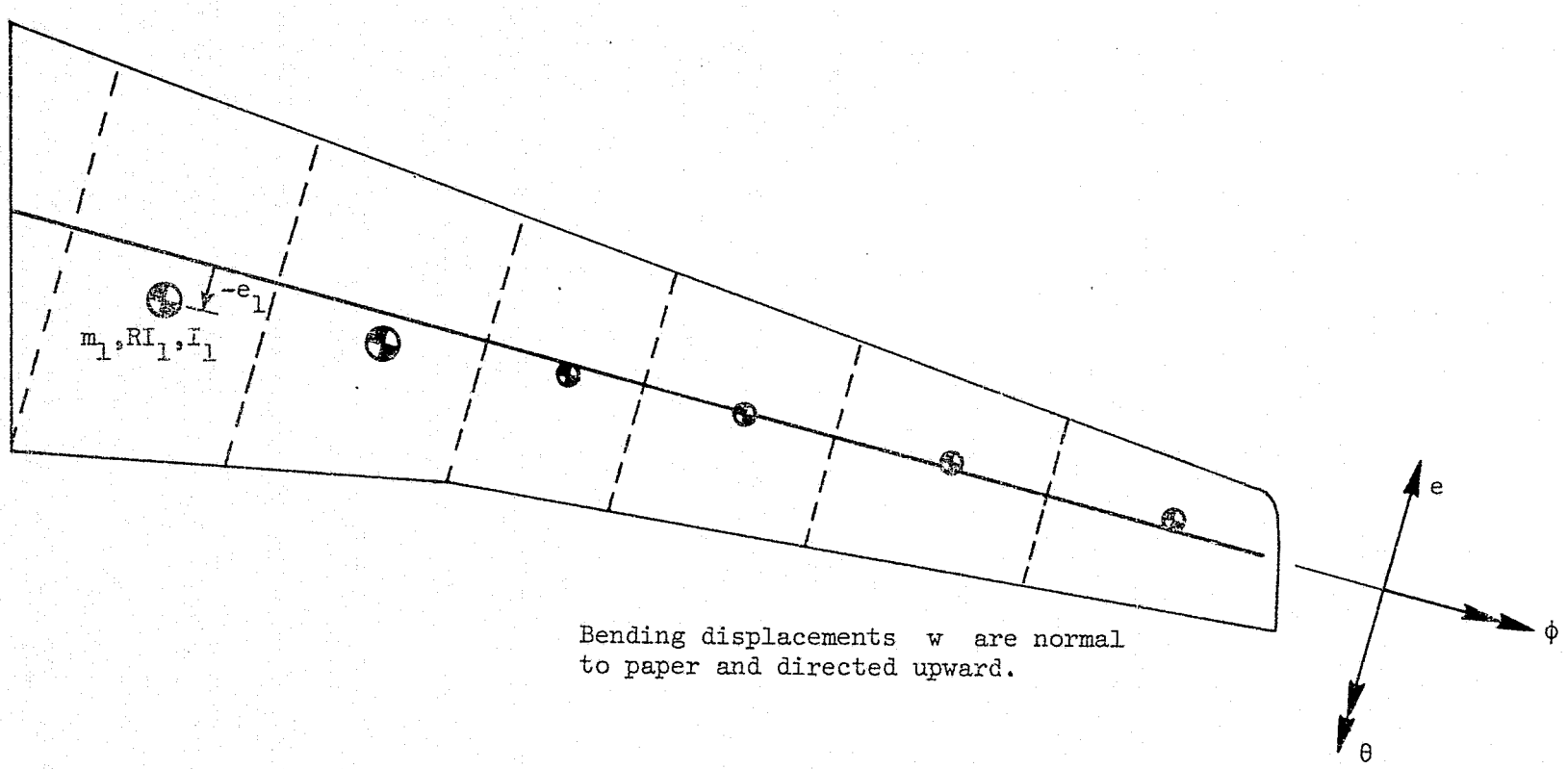

$$T_i = \frac{1}{2} m_i \left[w_i^2 \pm 2 e_i \dot{w}_i \dot{\phi}_i + \left(e_i \dot{\phi}_i \right)^2 \right] + \frac{1}{2} I_i \dot{\phi}_i^2 + \frac{1}{2} RI_i \dot{\theta}_i^2 \qquad i = 1,2,\ldots 6$$

Figure 8.- Identification of mass coupling terms arising from wing static unbalance.

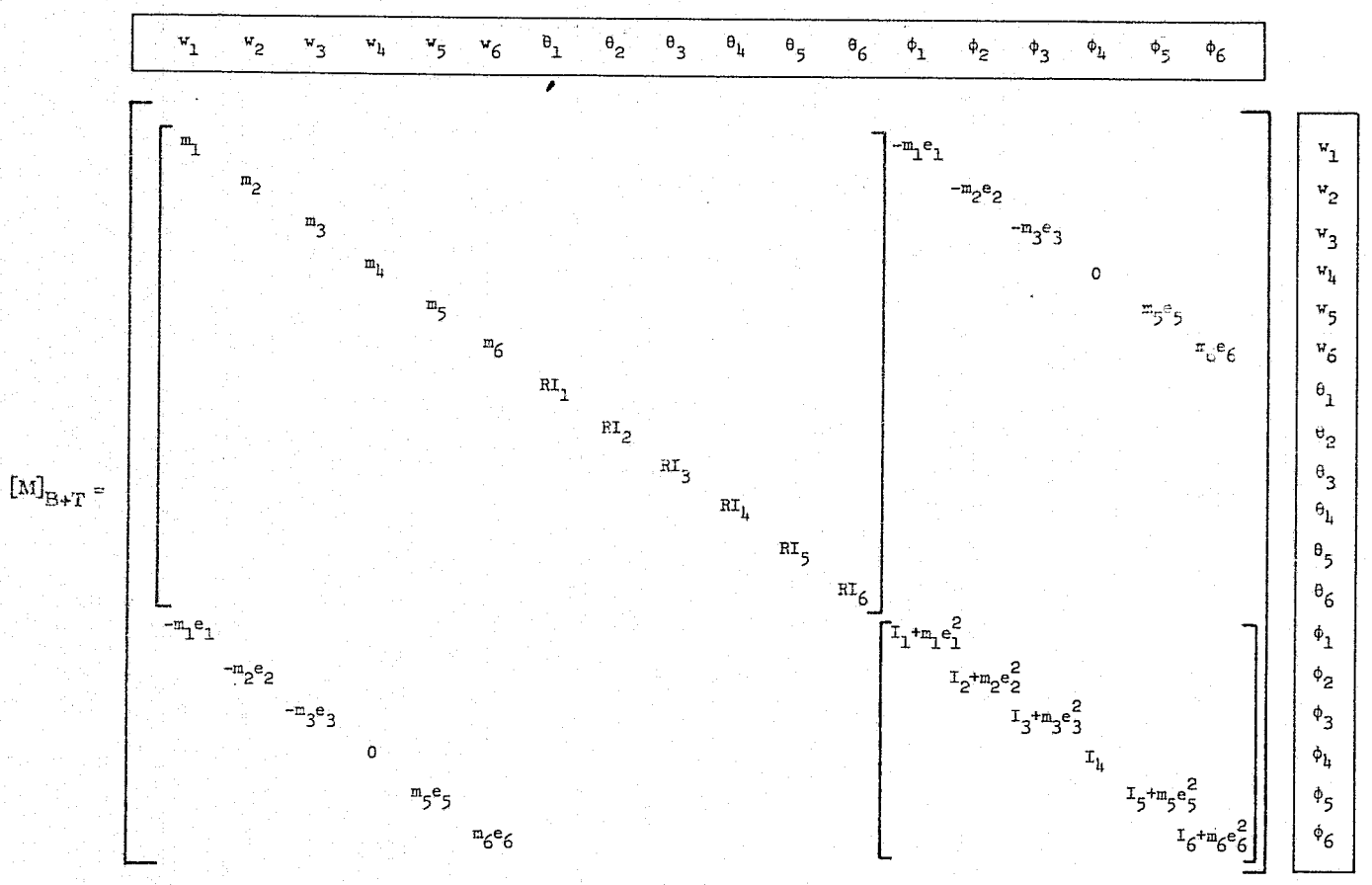

Figure 9.- Coupled bending-torsion mass matrix corresponding to the wing of figure 8.

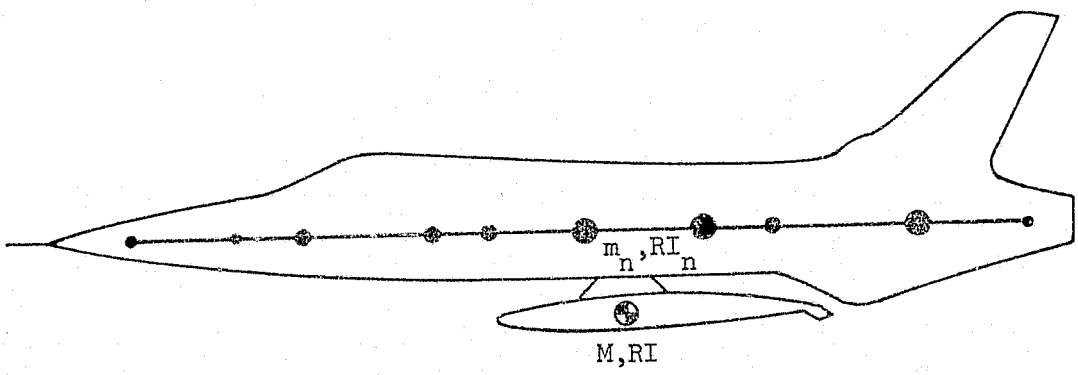

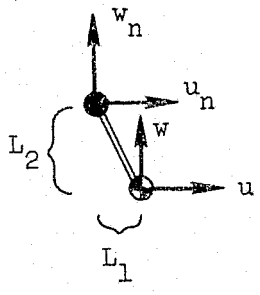

$$\dot{u} = \dot{u}_n + L_2\dot{\theta}_n \qquad \dot{w} = \dot{w}_n + L_1\dot{\theta}_n \qquad \dot{\theta} = \dot{\theta}_n$$

$$T = \frac{1}{2} M(\dot{u}^2 + \dot{w}^2) + \frac{1}{2} RI\ \dot{\theta}^2$$

$$T = \frac{1}{2} M(\dot{u}_n^2 + \dot{w}_n^2) + M(L_1\dot{\theta}_n\dot{w}_n + L_2\dot{\theta}_n\dot{u}_n) + \frac{1}{2}(RI + ML_1^2 + ML_2^2)\dot{\theta}_n^2$$

Figure 10.- Manner of accommodating the rigid-body inertial properties of a center-line fuel tank into the inertial matrix of the fuselage beam.

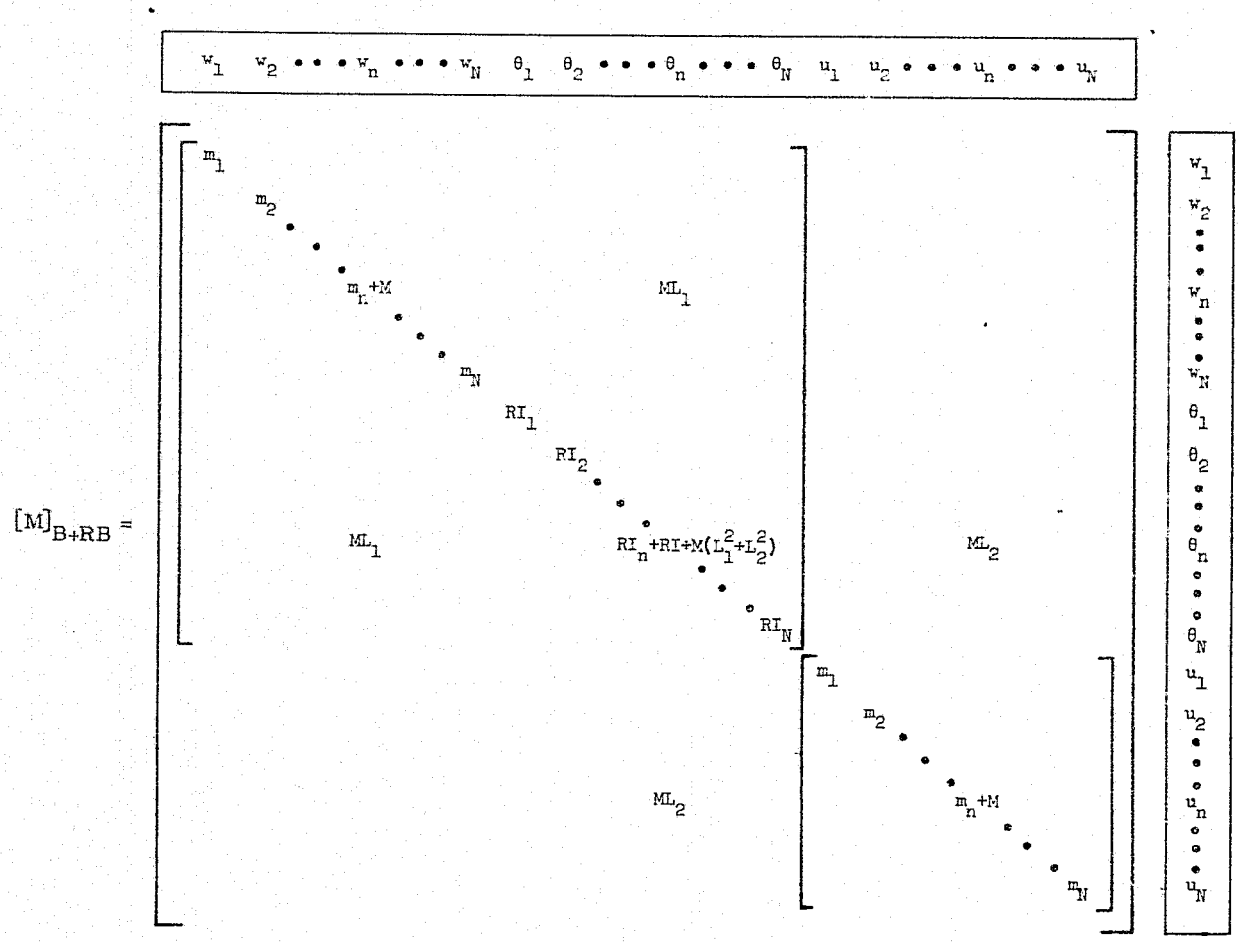

Figure 11.- Inertia matrix of the fuselage beam/fuel tank combination of figure 10.

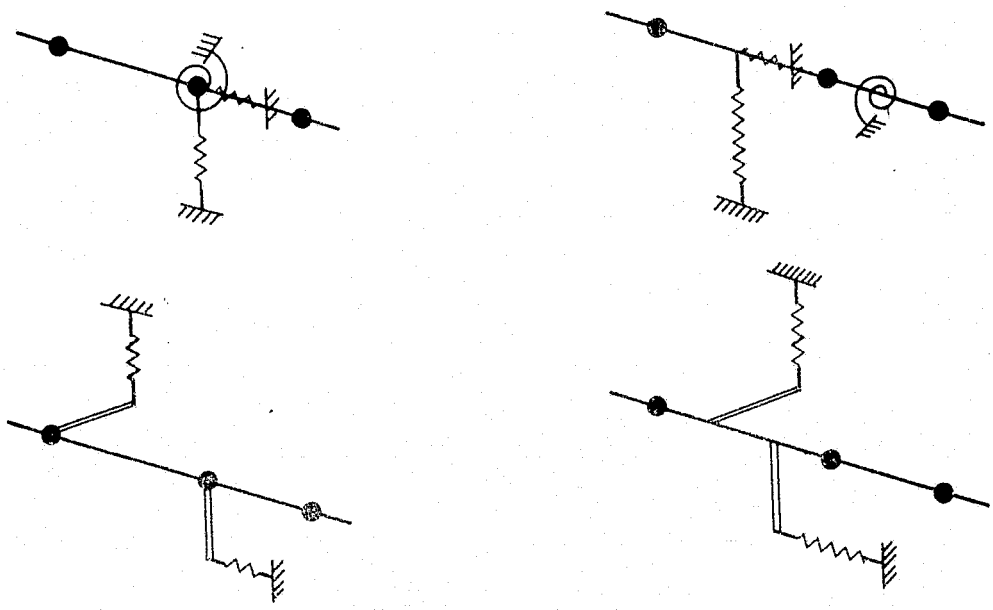

(a) Springs having one end tied to ground.

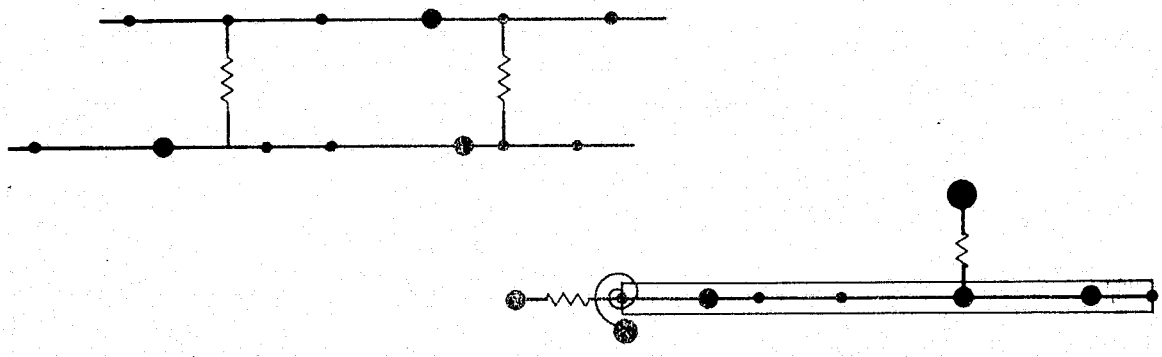

(b) Springs having both ends free to move.

Figure 12.- Some posible beam/spring arrangements which can arise from a structural idealization.

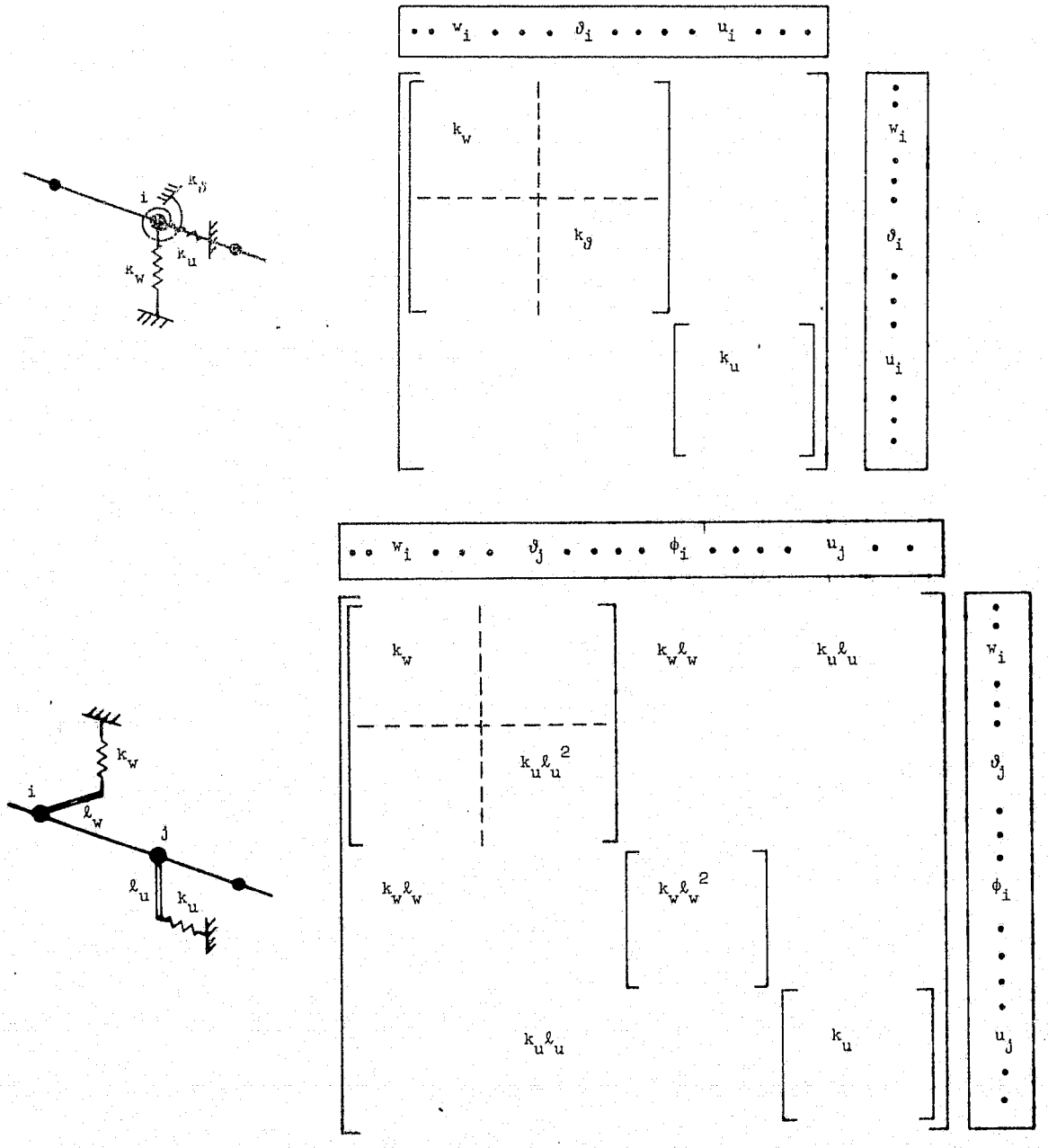

(a) Springs having one end tied to ground.

Figure 13.- Form of stiffness matrices corresponding to the spring components in several of the beam/spring arrangements of figure 12.

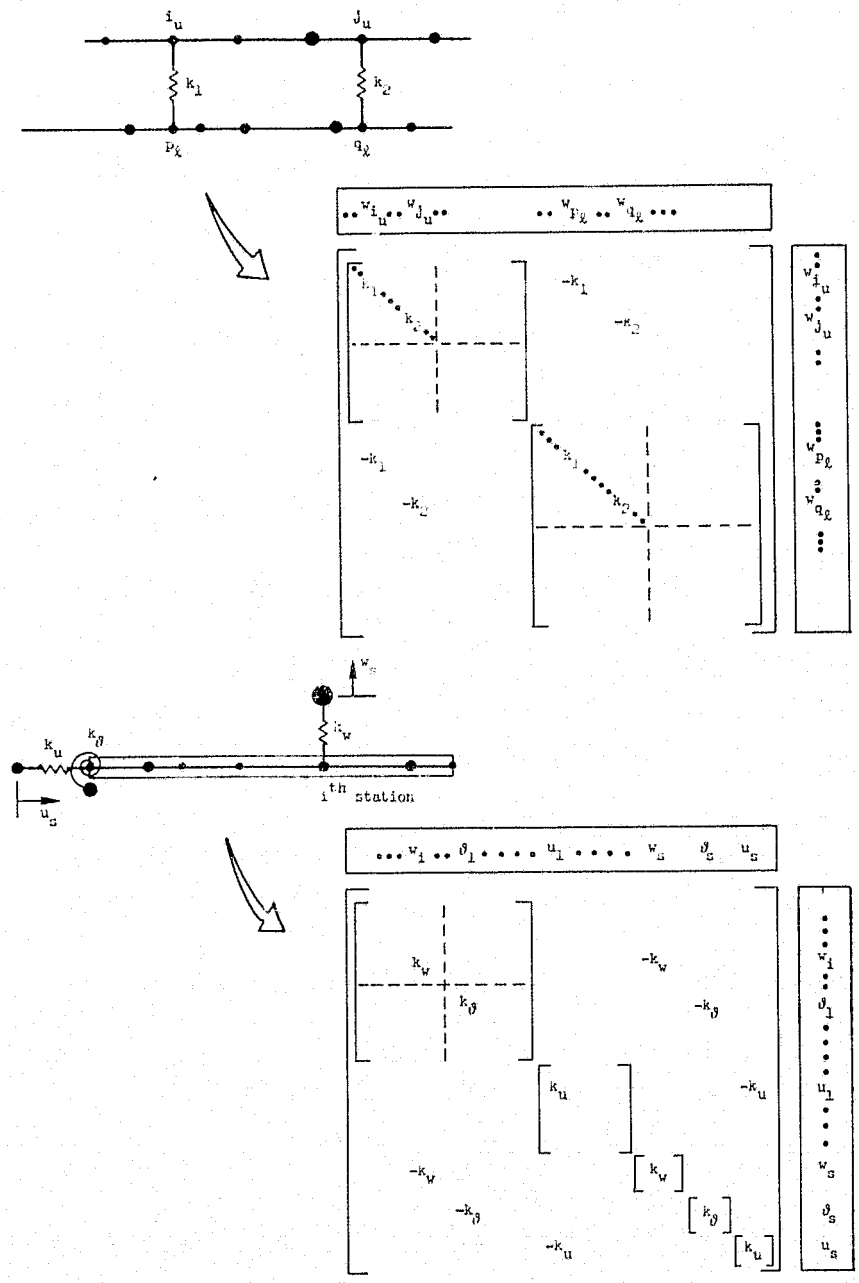

(b) Springs having both ends free to move.

Figure 13.- Concluded.

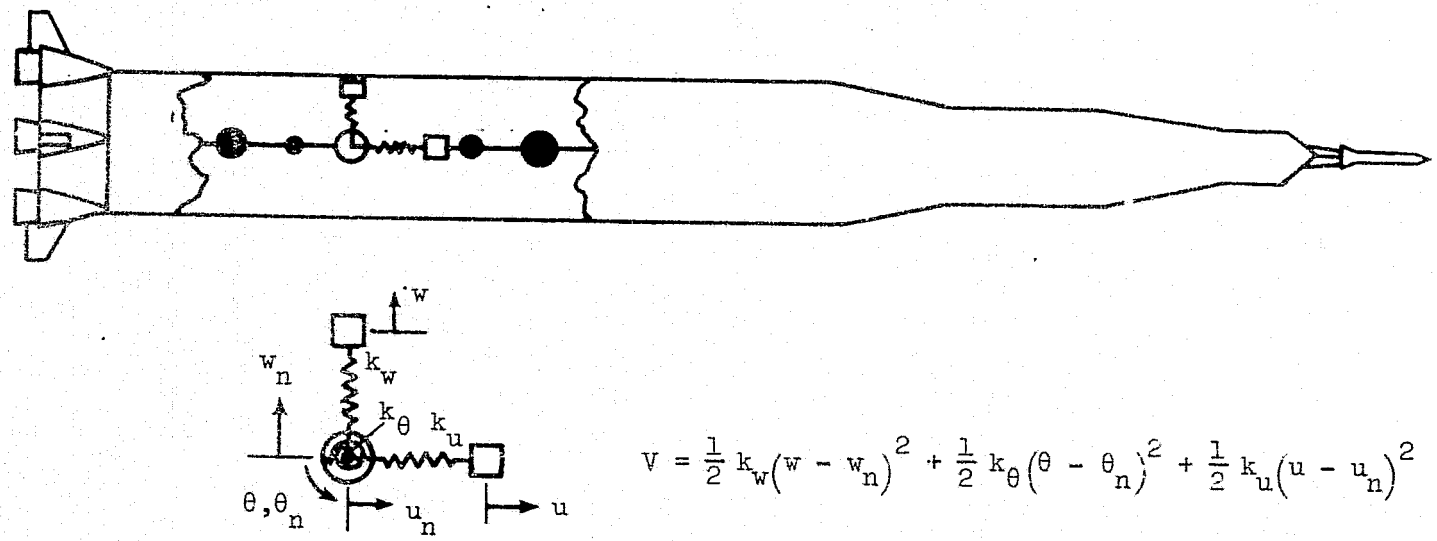

$$V = \frac{1}{2} k_w (w - w_n)^2 + \frac{1}{2} k_\theta (\theta - \theta_n)^2 + \frac{1}{2} k_u (u - u_n)^2$$

Figure 14.- Use of the spring-mass analogy to simulate the dynamics of sloshing propellant in a natural mode analysis.

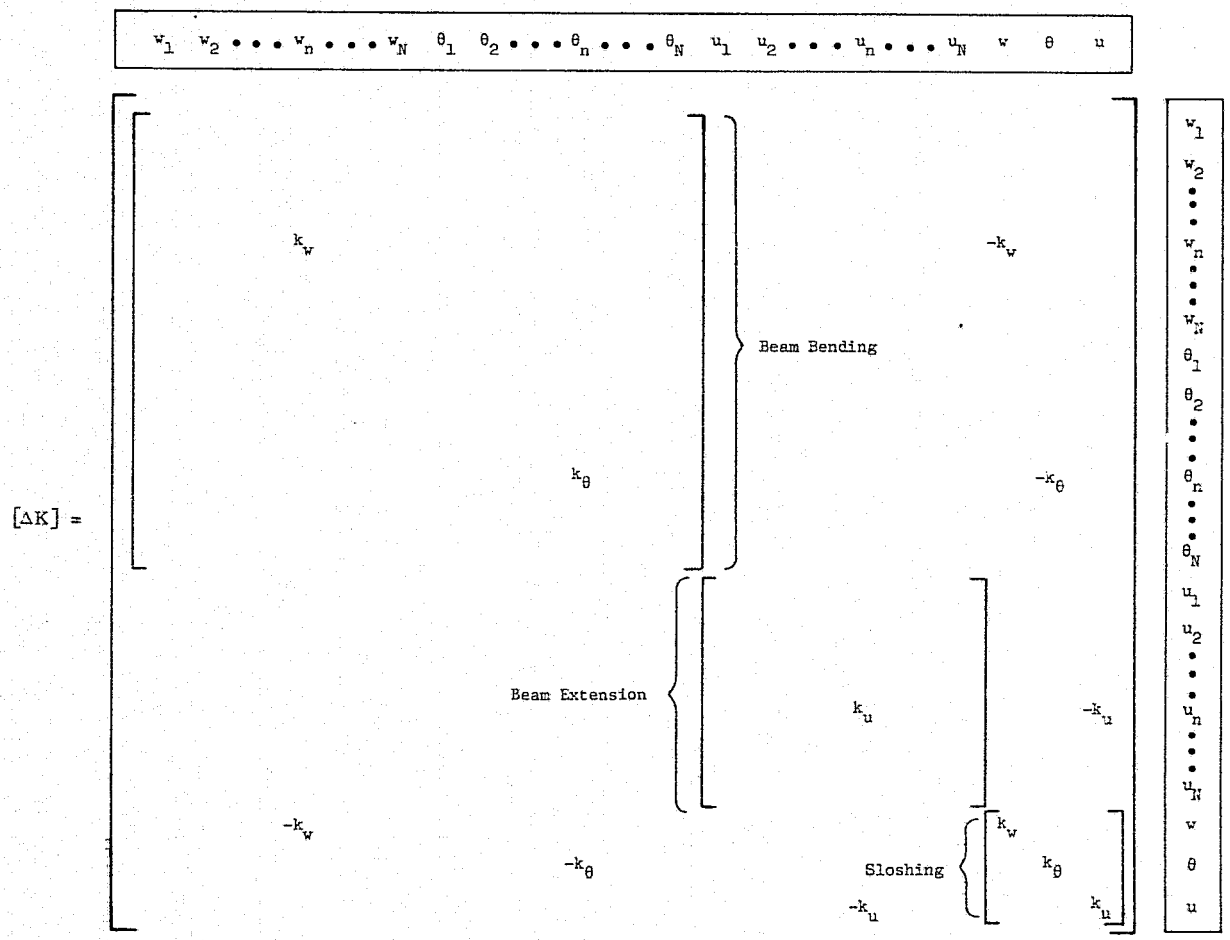

Figure 15.- Matrix of spring terms introduced by the spring-mass analogy of figure 14.

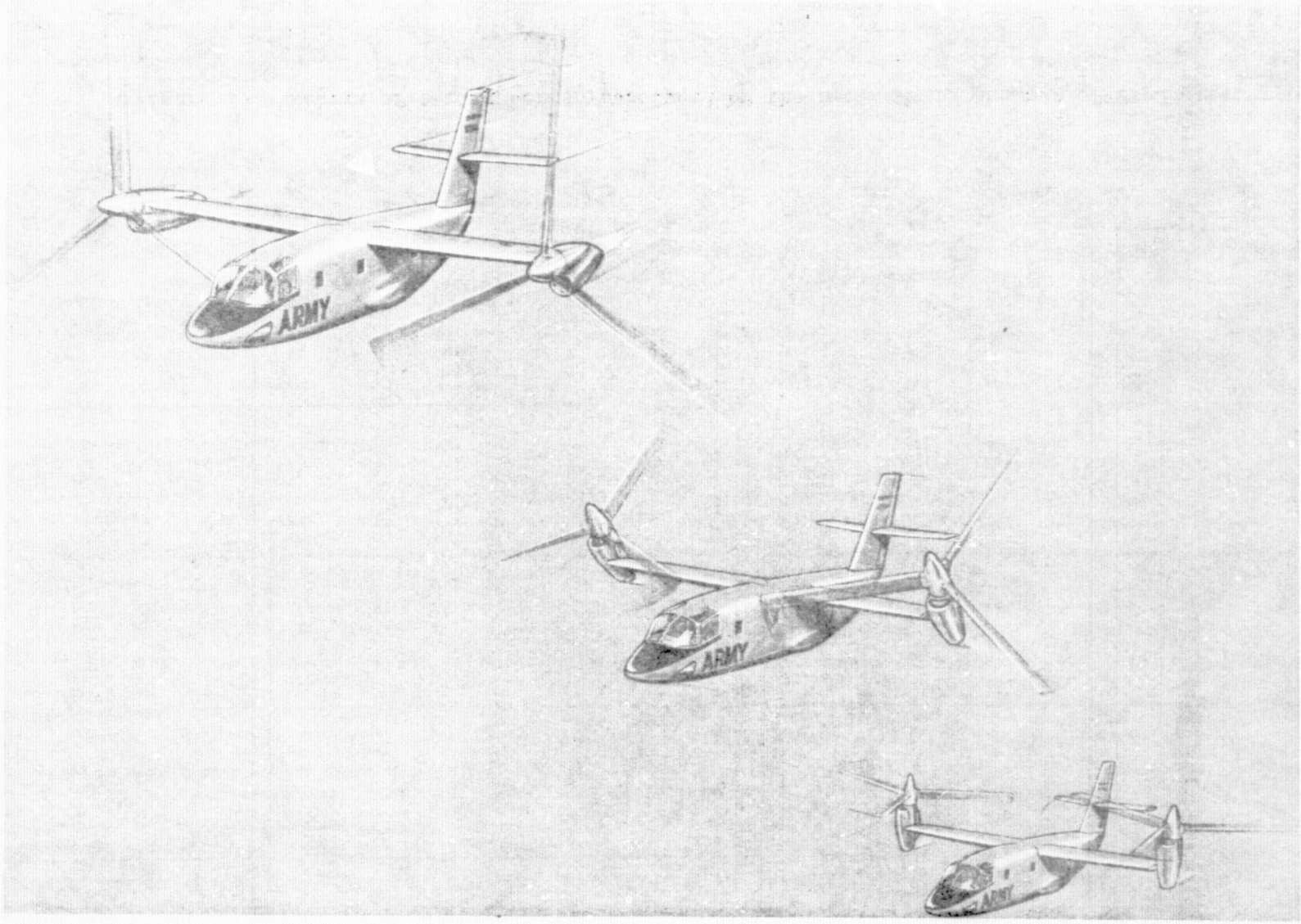

Figure 16.- Artist's conception of Bell Model 266 tilt-rotor VTOL aircraft.

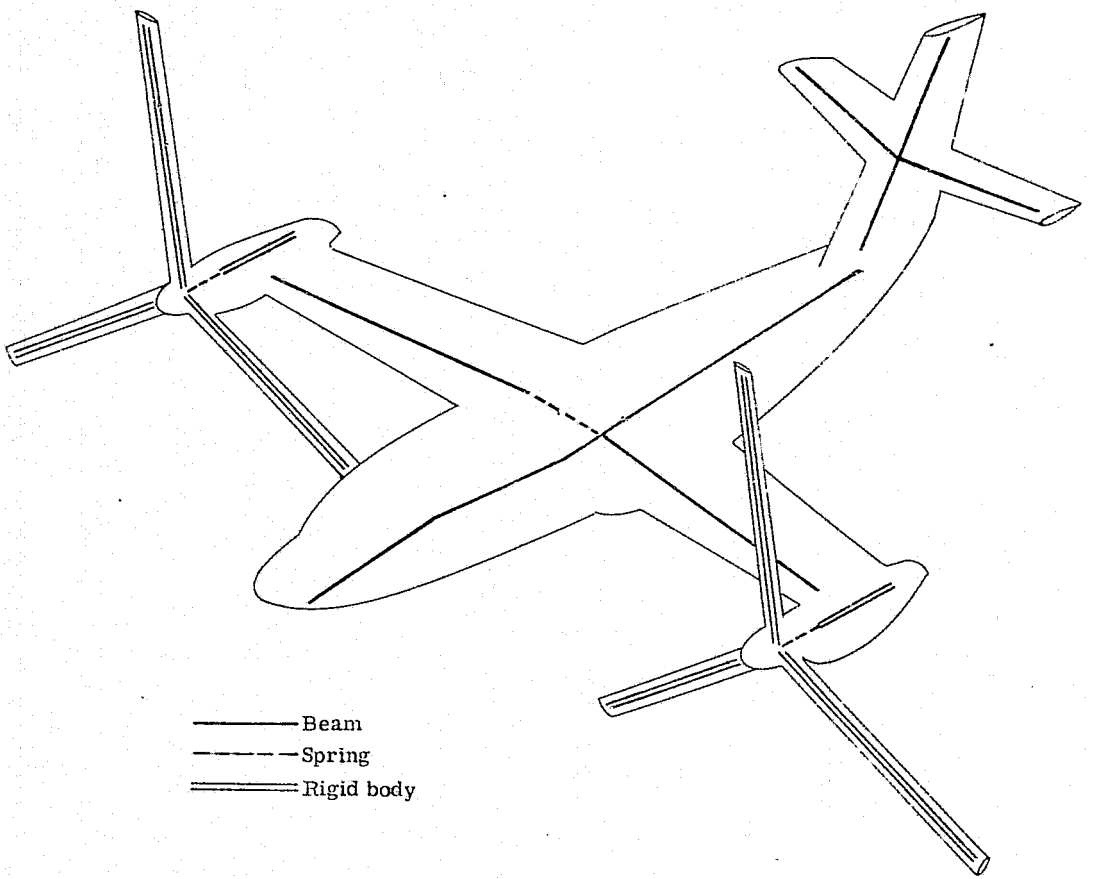

Figure 17.- Beam model of Bell Model 266 tilt-rotor aircraft.

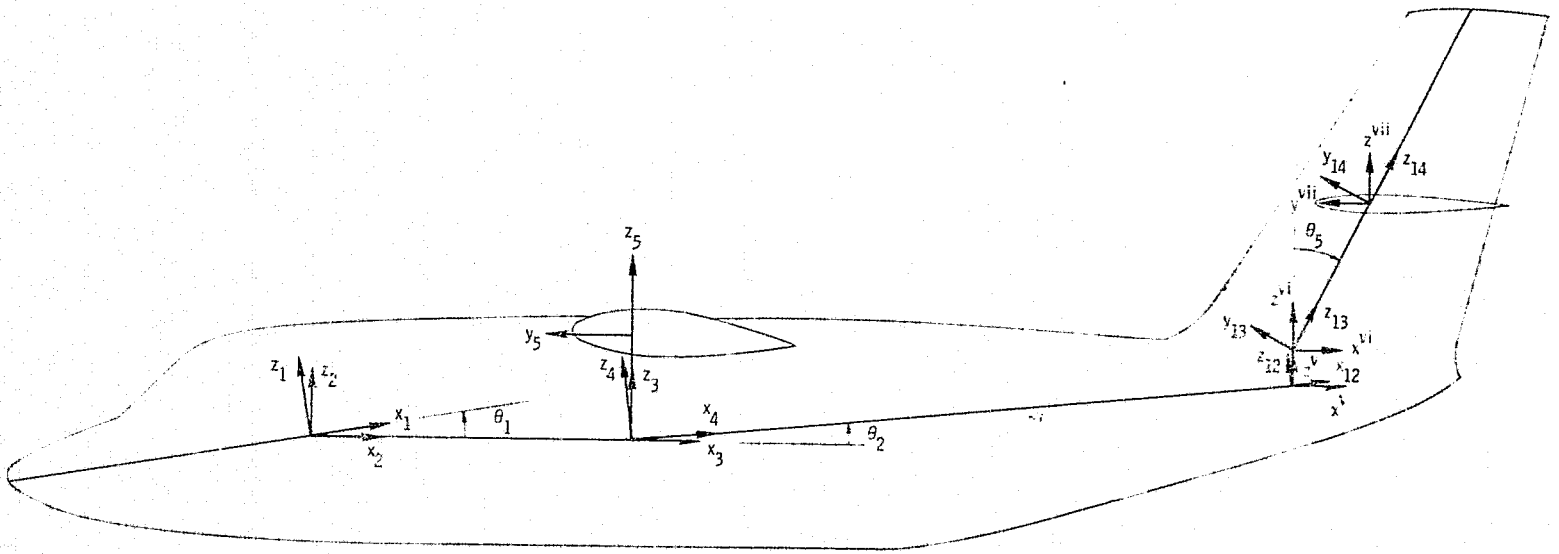

(a) Side view

Figure 18.- Coordinate systems used to write the equations of deflection compatibility between adjacent substructures.

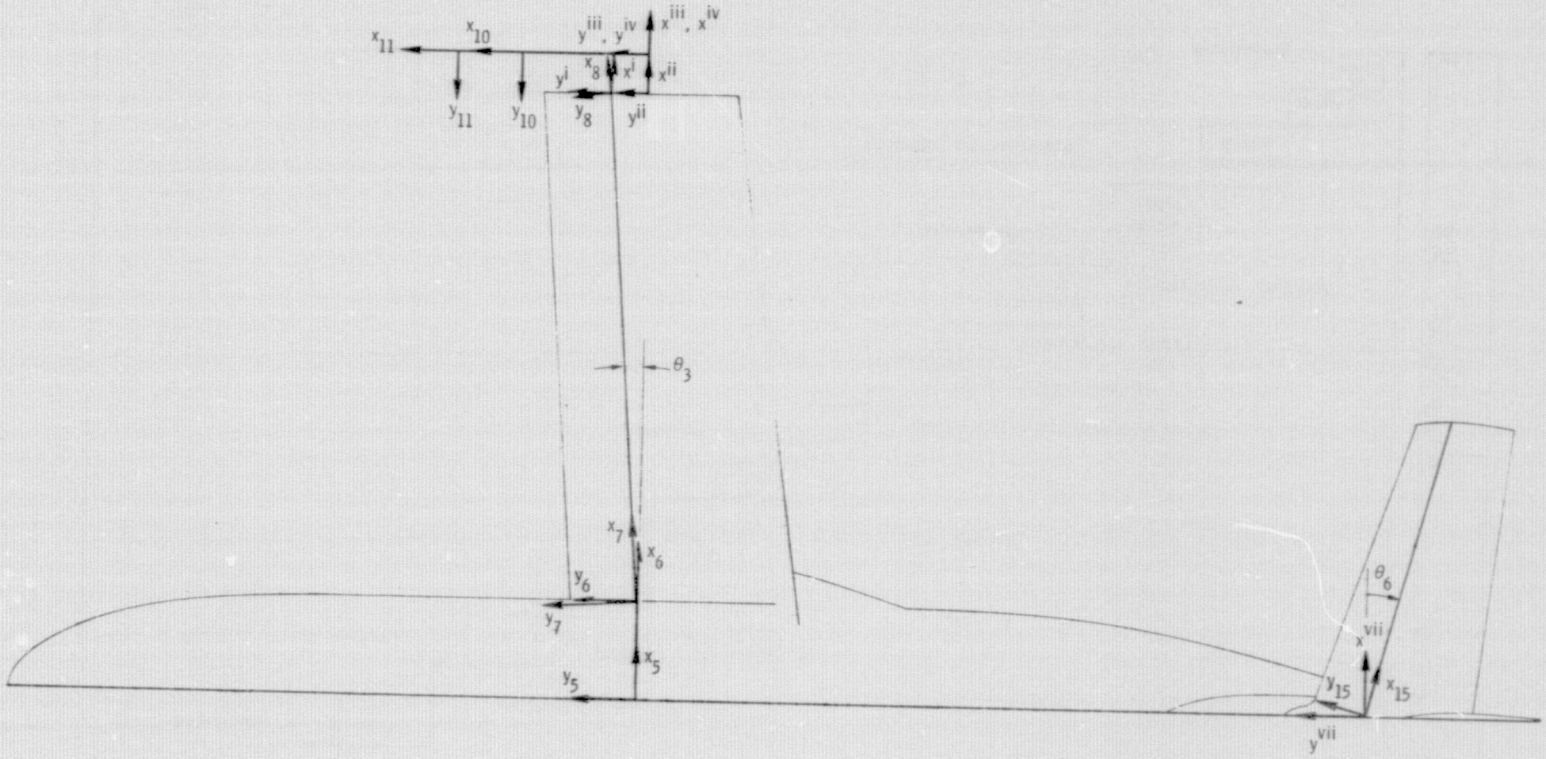

(b) Top view

Figure 18.- Concluded

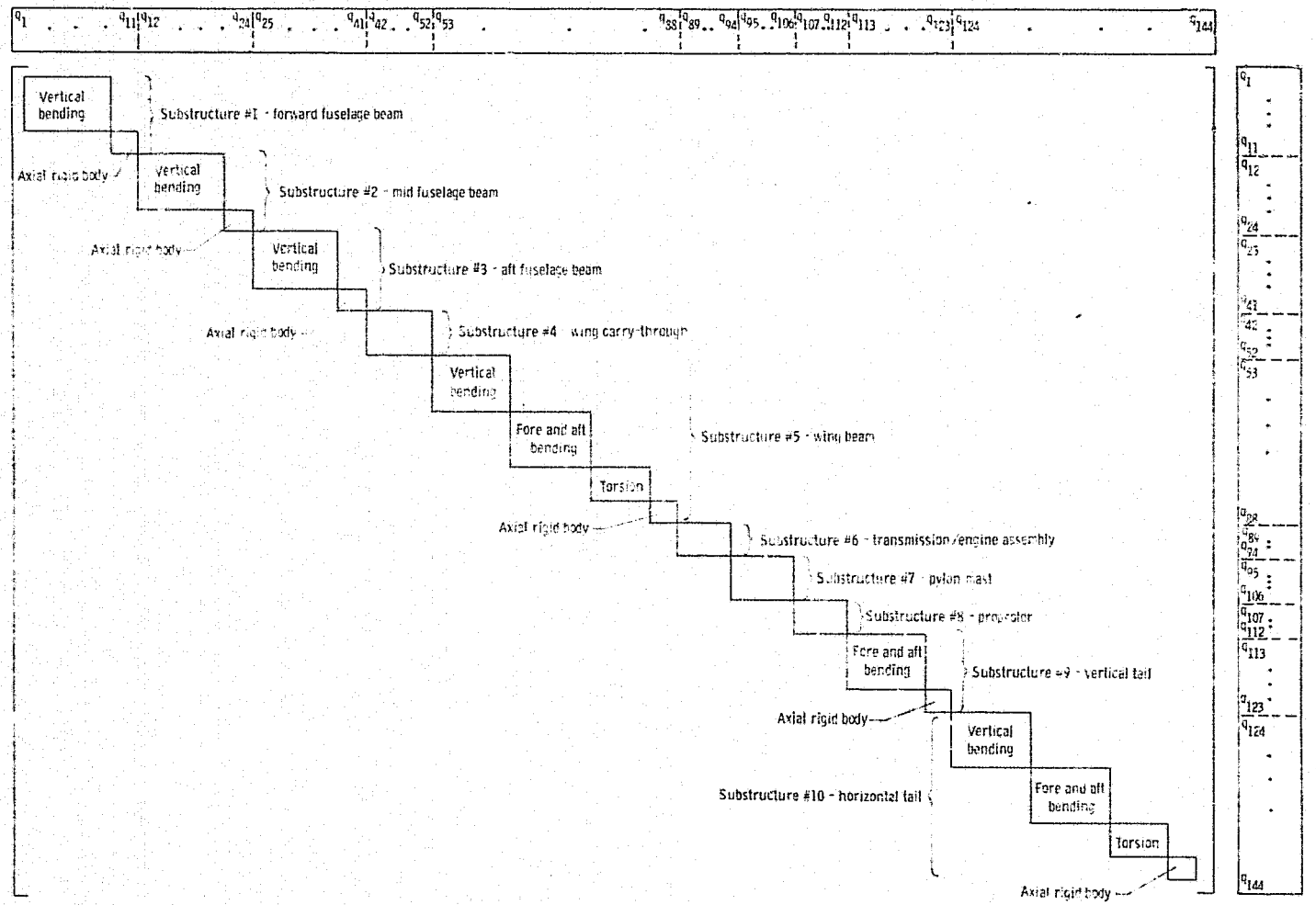

Figure 19.- Block composition of matrices $[\overline{M}]$ and $[\overline{K}]$ for symmetric analysis of beam model shown in figure 17.

$$[K]_{C\text{-}T} =$$

q_{42}	q_{43}	q_{44}	q_{45}	q_{46}	q_{47}	q_{48}	q_{49}	q_{50}	q_{51}	q_{52}	
$\frac{12EI_z}{L^3}$	0	0	0	$\frac{6EI_z}{L^2}$	0	$-\frac{12EI_z}{L^3}$	0	0	0	$\frac{6EI_z}{L^2}$	q_{42}
	$\frac{12EI_y}{L^3}$	0	$-\frac{6EI_y}{L^2}$	0	0	0	$-\frac{12EI_y}{L^3}$	0	$-\frac{6EI_y}{L^2}$	0	q_{43}
		$\frac{GJ}{L}$	0	0	0	0	0	$-\frac{GJ}{L}$	0	0	q_{44}
			$\frac{4EI_y}{L}$	0	0	0	$\frac{6EI_y}{L^2}$	0	$\frac{2EI_y}{L^2}$	0	q_{45}
				$\frac{4EI_z}{L}$	0	$-\frac{6EI_z}{L^2}$	0	0	0	$\frac{2EI_z}{L}$	q_{46}
					$\frac{AE}{L}$	0	0	0	0	0	q_{47}
						$\frac{12EI_z}{L^3}$	0	0	0	$-\frac{6EI_z}{L^2}$	q_{48}
			Symmetric				$\frac{12EI_y}{L^3}$	0	$\frac{6EI_y}{L^2}$	0	q_{49}
								$\frac{GJ}{L}$	0	0	q_{50}
									$\frac{4EI_y}{L}$	0	q_{51}
										$\frac{4EI_z}{L}$	q_{52}

Figure 20.- Stiffness matrix of wing carry-through beam-spring for symmetric vibration analysis.

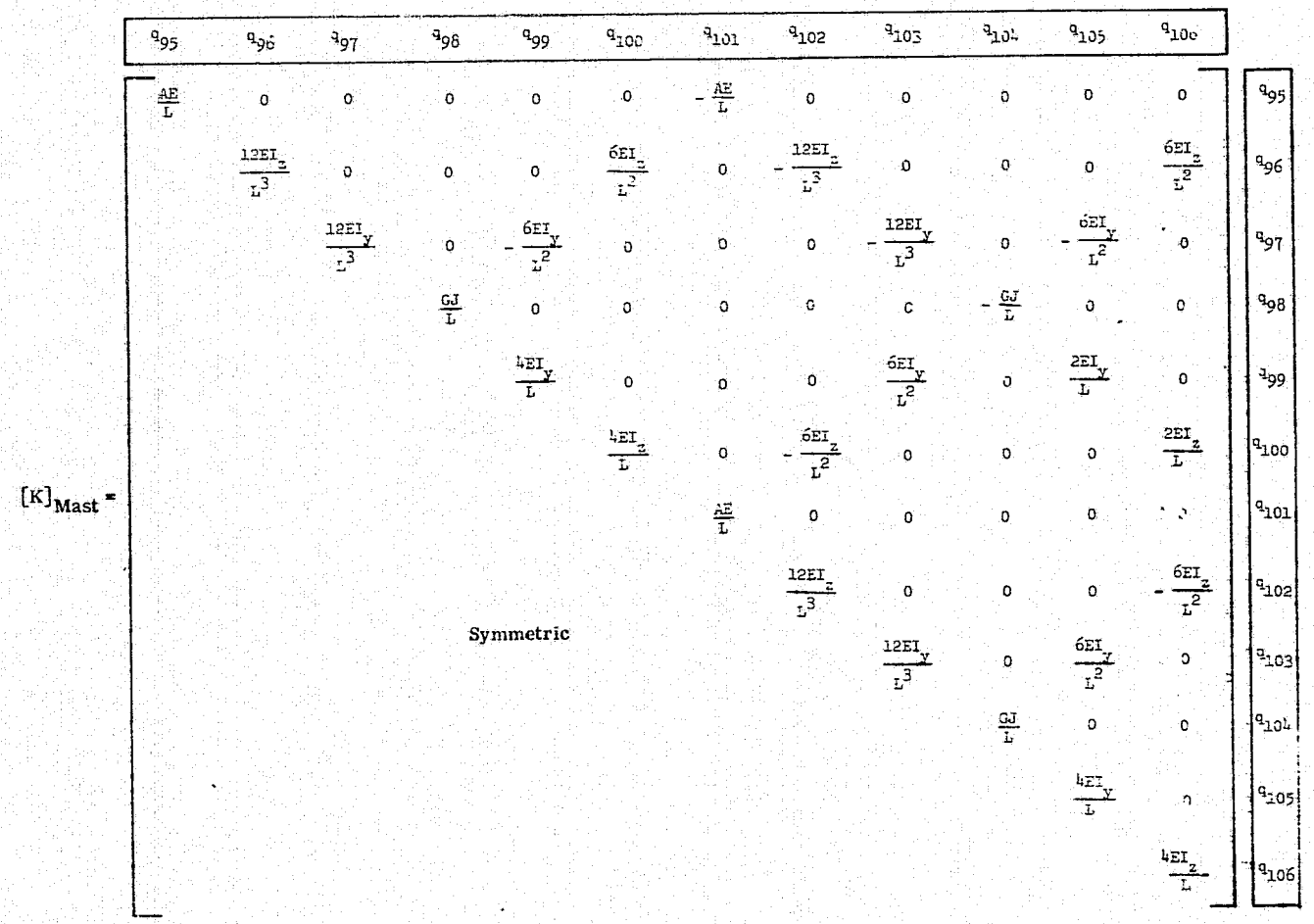

Figure 21.- Stiffness matrix of pylon mast beam-spring for symmetric vibration analysis.

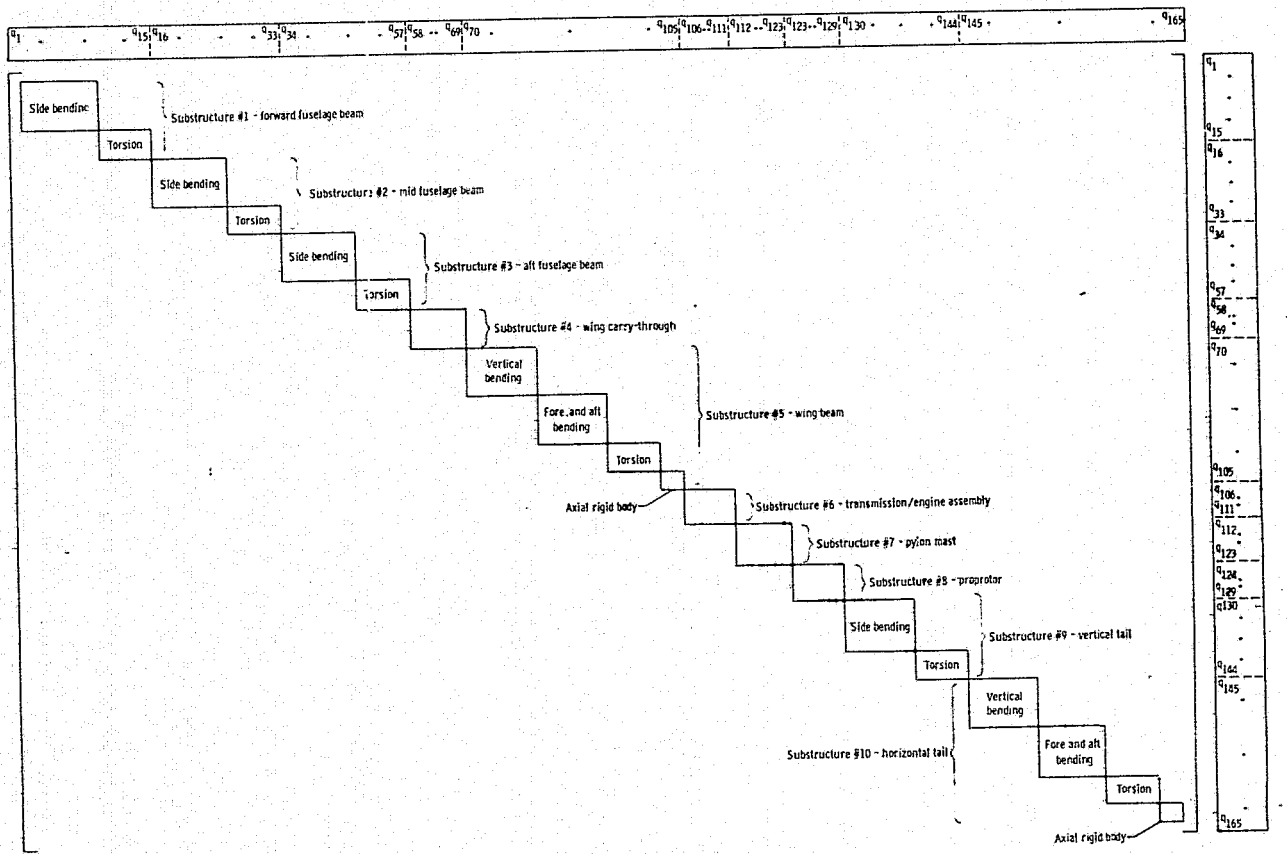

Figure 22.- Block diagonal composition of $[\overline{M}]$ and $[\overline{K}]$ for anti-symmetric analysis of beam model shown in figure 17.

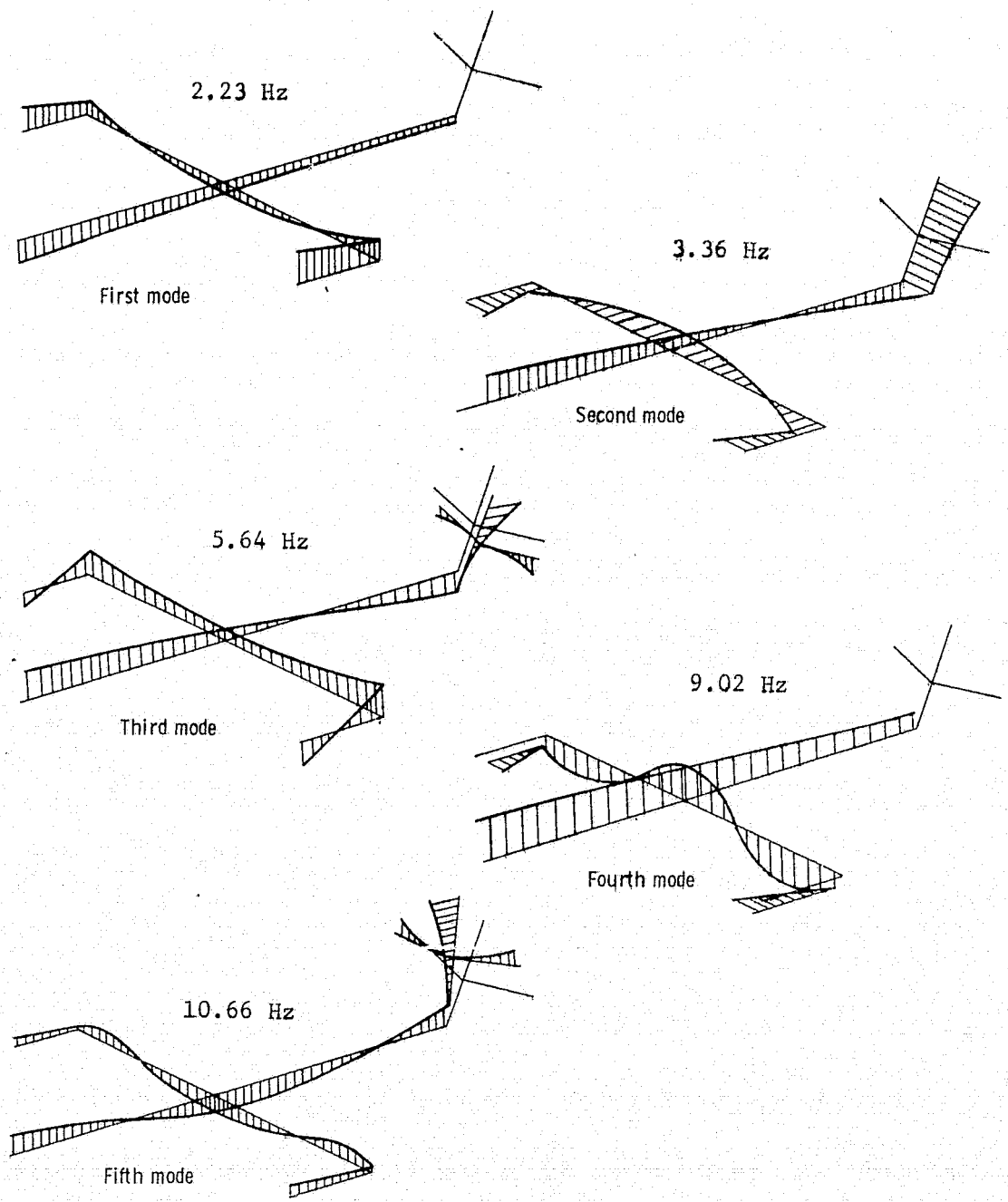

Figure 23.- First five symmetric elastic modes of Model 266 tilt-rotor ($\theta_c = 90^\circ$).